FORMATION AND CHARACTERIZATION OF ELECTROFORMED CYLINDRICAL ACCORDION GEOMETRY

A THESIS SUBMITTED TO
THE GRADUATE SCHOOL OF NATURAL AND APPLIED SCIENCES
OF
MIDDLE EAST TECHNICAL UNIVERSITY

BY

BİLGEHAN ÇETİNÖZ

IN PARTIAL FULFILLMENT OF THE REQUIREMENTS
FOR
THE DEGREE OF MASTER OF SCIENCE
IN
METALLURGICAL AND MATERIALS ENGINEERING

FEBRUARY 2018

Approval of the thesis:

FORMATION AND CHARACTERIZATION OF ELECTROFORMED CYLINDRICAL ACCORDION GEOMETRY

submitted by **BİLGEHAN ÇETİNÖZ** in partial fulfillment of the requirements for the degree of **Master of Science in Metallurgical and Materials Engineering Department, Middle East Technical University** by,

Prof. Dr. Gülbin Dural Ünver _____
Dean, Graduate School of **Natural and Applied Sciences**

Prof. Dr. Cemil Hakan Gür _____
Head of Department, **Metallurgical and Materials Engineering**

Prof. Dr. İshak Karakaya _____
Supervisor, **Metallurgical and Materials Eng. Dept., METU**

Assist. Prof. Dr. Metehan Erdoğan _____
Co-Supervisor, **Materials Eng. Dept., AYBU**

Examining Committee Members:

Prof. Dr. Kadri Aydınol _____
Metallurgical and Materials Engineering Dept., METU

Prof. Dr. İshak Karakaya _____
Metallurgical and Materials Engineering Dept., METU

Assist. Prof. Dr. Metehan Erdoğan _____
Materials Eng. Dept., Ankara Yıldırım Beyazıt University

Assist. Prof. Dr. Batur Ercan _____
Metallurgical and Materials Engineering Dept., METU

Assist. Prof. Dr. Erkan Konca _____
Metallurgical and Materials Eng. Dept., Atılım University

Date: *02/02/2018*

I hereby declare that all information in this document has been obtained and presented in accordance with academic rules and ethical conduct. I also declare that, as required by these rules and conduct, I have fully cited and referenced all material and results that are not original to this work.

Name, Last name: Bilgehan Çetinöz Signature:

ABSTRACT

FORMATION AND CHARACTERIZATION OF ELECTROFORMED CYLINDRICAL ACCORDION GEOMETRY

Çetinöz, Bilgehan
M.S., Department of Metallurgical and Materials Engineering
Supervisor: Prof. Dr. İshak Karakaya
Co-supervisor: Assist. Prof. Dr.Metehan Erdoğan February
2018, 69 pages

Highly complicated cylindrical accordion geometry was produced by electroforming method. Additive free nickel sulphamate bath was used to obtain nickel electrodeposition within the scope of this study. Pulse-reverse current method was applied to enhance mechanical and surface properties of nickel electrodeposition. Average current density, peak current density and the ratio of cathodic to anodic current densities were optimized to get better electroform. Scanning electron microscope images, hardness measurements and the results of x-ray diffraction analyses were evaluated to get information about microstructure of nickel electrodeposition.

In addition, removal of nickel chloride from the electrolyte and the use of S-anode instead of high purity nickel anode were investigated to decrease internal stress and get better anode efficiency. Furthermore, elasticity of accordion shape nickel electroform was improved by heat treatment.

Keywords: Pulse-reverse plating, electroplating, nickel electrodeposition, bellow, electroforming

ÖZ

SİLİNDRİK AKORDİYON GEOMETRİSİNİN

ELEKTROFORM YÖNTEMİ İLE OLUŞTURULMASI VE KARAKTERİZASYONU

Çetinöz, Bilgehan

Yüksek Lisans, Metalurji ve Malzeme Mühendisliği Bölümü

Tez Yöneticisi: Prof. Dr. İshak Karakaya

Ortak Tez Yöneticisi: Yrd. Doç. Dr. Metehan Erdoğan

Şubat 2018, 69 sayfa

Elektroform metodu kullanılarak oldukça karmaşık silindirik akordiyon geometri elde edildi. Çalışma kapsamında katkı maddesiz nikel sülfamat banyosu kullanıldı. Darbeli-ters akım yöntemi uygulanarak nikel elektrokaplamanın mekanik ve yüzey özellikleri geliştirildi. Ortalama akım yoğunluğu, tepe akımı yoğunluğu ve katodik akım yoğunluğunun anodik akım yoğunluğuna oranı optimize edildi Taramalı elektron mikroskop görüntüleri, sertlik ölçümleri ve x-ray kırınım çözümlemesi analiz sonuçları değerlendirilerek, nikel elektrokaplamanın mikro yapısı hakkında bilgi edinildi.

Ek olarak, iç gerilimi azaltmak ve akım verimliliğini artırmak için, nikel klorür elektrolitten çıkarıldı ve yüksek saflıktaki nikel anot yerine S-anot kullanıldı. Ayrıca, akordiyon şeklindeki nikel elektroformun elastikliği ısıl işlem uygulanarak geliştirildi.

Anahtar kelimeler: Darbeli-ters kaplama, elektrokaplama, nikel elektrokaplama, körük, elektroform

To my family

ACKNOWLEDGEMENTS

I would like to express my deepest gratitude to my advisors Prof. Dr. İshak Karakaya and Assist. Prof. Dr.Metehan Erdoğan for their patience, motivation, guidance, advice, criticism, support and insight not only throughout this thesis but in many other studies. I could not have imagined having better advisors for my master study.

Many thanks go to Büşra Aykaç, Mertcan Başkan, Esra Karakaya, Çağlar Polat and Olgun Yılmaz for their support and assistance throughout this thesis. I must express my very profound gratitude to Mustafa Serdal Aras for providing me with unfailing support and continuous encouragement throughout my years of study.

My special thanks goes to Mustafa Anıl Yıldırım for his never ending friendship and support. I could not have adapted quickly to this sudy and METU.

Finally, I would like to acknowledge the technical and the financial support of ASELSAN Incorporation and MEGAP Co. Ltd.

TABLE OF CONTENTS

ABSTRACT v
ÖZ vi
ACKNOWLEDGEMENTS ix
LIST OF TABLES 13
LIST OF FIGURES 14

CHAPTERS

1. INTRODUCTION 1

1.1 Production of Micron Size Engineering Metal Parts 1

1.2 The Purpose of The Thesis 3

2. LITERATURE REVIEW 5

2.1 Fundamental Concepts of Electrodeposition 5

2.2 Cell Types of The Electrochemistry 6

2.3 Nickel Electrodeposition 12

2.3.1 Anode Passivation 14

2.3.2 Hydrogen Evolution 15

2.3.3 pH Changes 16

2.3.4 Non-Equal Current Distribution 16

2.4 Pulse-Reverse Current Method 17

2.4.1 Working principle of the Pulse reverse method 18

2.4.2 Effect on Microstructure 20

2.4.3 Effect on Mechanical Properties 20

3. EXPERIMENTAL PROCEDURE 23

3.1 Coupon Based Experiments 24

3.1.1 Pretreatments 24

3.1.2 Preparing Electrolyte 25

3.2 Experiments to form Accordion Geometry 27

3.2.1 Pretreatments 27

3.2.2 Cell Design and Electrodeposition 30

4. RESULTS AND DISCUSSION 33

4.1 Application of DC, PC and PRC Methods 33

4.2 Effect of Average Current Density on Microstructure and Hardness 37

4.3 Effect of Peak Current Density on Microstructure and Hardness 41

4.4 The Effects of Anodic to Cathodic Current Ratio on Microstructure and Hardness 44

4.5 Introduction of Elastic Properties 47

4.5.1 Use of S-Anodes in Non-chloride Sulphamate Bath 47

4.5.2 Ni-Co Alloy Plating and Heat Treatment 55

5. CONCLUSIONS 61

REFERENCES 63

LIST OF TABLES

TABLES

Table 1 Bath contents and working conditions of sulphamate baths[19] 15

Table 2 Operating conditions and composition of nickel sulphamate bath 26

Table 3 The parameters used to study pulse-reverse nickel electrodeposition..... 28

Table 4 Copper pyrophosphate strike bath composition and operating conditions [43] 31

Table 5 Studied parameters for accordion geometry 31

Table 6 Thickness measurements of nickel electroform with different anodic to cathodic current ratio ..... 50 Table 7 Coupon based experiments employing S-anode 52

Table 8 The results of tensile tests for electroformed Ni-Co alloys heat treated at different temperatures 58

LIST OF FIGURES

FIGURES

Figure 1 Nickel mould for wing skins of Harrier. Reproduced from [4]..... 3

Figure 2 Different bellow shapes Reproduced from [5] 4

Figure 3 A schematic representation of electrodeposition cell 5

Figure 4 Cell types (a) Galvanic and (b) Electrolytic cells..... 7

Figure 5 Idealized Tafel Plot [13] 10

Figure 6 Cathode-electrolyte interfe a) equilibrium, b) and c) deviations from equilibrium [15] 11

Figure 7 Comparison of internal stress of nickel coatings on bath type and current density [21] 13

Figure 8 Effects of throwing power a) low b) high throwing power 14

Figure 9 Examples of non-uniform current distributions in electroplating [29]..... 17

Figure 10 Pulse-reverse bipolar current wave shape [33]..... 18

Figure 11 The change of concentration with time in DC and PC [34] 19

Figure 12 Schematic drawing of a copper coupon and the pretreatment process for cathode 25

Figure 13 A photograph of the cell used in coupon based experiments 27

Figure 14 Zincate treatment for aluminum mandrel 29

Figure 15 Picture of experimental set-up for plating accordion geometry 32

Figure 16 Computer simulation of electroformed bellow by DC method 33

Figure 17 SEM images of nickel electrodeposition by (a) DC (b) PC (I_{ON}=5A/dm^2 , t_{ON}= 2 ms, t_{OFF}= 3 ms) and (c) PRC (I_{CC}=20 A/dm^2, t_{CC}= 3 ms, I_{AA}=20 A/dm^2, t_{AA}=1 ms and t_{OFF}=16 ms) method at a current density of 2 A/dm^2. The scale at the bottom applies to all. 35

Figure 18 XRD results of nickel electrodeposition with DC and PRC methods 36

Figure 19 SEM images of nickel electrodeposition (a) DC (2 A/dm^2) (b) PRC (I_{CC}=5 A/dm^2, t_{CC}= 3 ms, I_{AA}=2 A/dm^2, t_{AA}=1 ms and t_{OFF}=2.5 ms) 36

Figure 20 The surface of nickel electrodeposition by a) DC (1.5 A/dm^2) and b)PRC method (I_{CC}=20 A/dm^2, t_{CC}= 0.3 ms, I_{AA}=20 A/dm^2, t_{AA}=0.1 ms and t_{OFF}=2.3 ms) 37

Figure 21 Microstructures of nickel electrodeposited at average current densities of; a) 1 A/dm^2, b) 3 A/dm^2, and c) 5 A/dm^2 at different magnifications 39

Figure 22 XRD results of nickel electrodeposited at different average current densities 40

Figure 23 Hardness values of nickel electrodeposited at different average current densities 40

Figure 24 Images of nickel electrodeposition at; a) 1 A/dm^2 and b) 5 A/dm^2 average current densities 41

Figure 25 SEM images of nickel electrodepositions at different peak current densities; a.) 40 A/dm^2, b.) 70 A/dm^2, c.) 120 A/dm^2 The scale at the top applies to all. 42

Figure 26 XRD results of nickel electrodeposited samples at different peak current densities 43

Figure 27 Hardness measurements of electrodeposited nickel at different peak current densities 44

Figure 28 Hardness of nickel electrodepositions for different anodic to cathodic current ratios 46

Figure 29 SEM images of of nickel electrodeposition when a) $\frac{\text{anodic current}}{\text{cathodic current}}=0.6$, b) $\frac{\text{cathodic current}}{\text{anodic current}}=0.6$..... 46

Figure 30 The X-ray diffraction of nickel electrodeposition at cathodic to anodic current ratios of; a) $\frac{\text{anodic current}}{\text{cathodic current}}=0.6$ and b) $\frac{\text{cathodic current}}{\text{anodic current}}=0.6$..... 48

Figure 31 The cross section of the nickel accordion geometry for different ratios of anodic current to cathodic current a) 0.1, b) 0.5 and c) 1 49

Figure 32 The thickness distribution of nickel electrodeposits when the mask and PRC (I_{CC}= 20 A/dm^2, t_{CC}= 0.3 ms, I_{AA}= 10 A/dm^2, t_{AA}=0.1 ms and t_{off}= 2.8 ms) were used together 50

Figure 33 SEM images of nickel electrodeposits at different t_{off} (a) 24 ms (b) 21ms (c) 18 ms (d) 15 ms (e) 12 ms and (f) 9 ms The scale at the top applies to all given at two different magnifications ..... 54 Figure 34 Hardness values of nickel electrodeposits for different off times 55

Figure 35 Tensile test specimens for Ni-Co alloys 56

Figure 36 Tensile stress vs strain graphs of 3% Cobalt alloy heat treated at different temperatures 59

Figure 37 Tensile stress vs strain graphs of 4% Cobalt alloy heat treated at different temperatures 60

CHAPTER 1

INTRODUCTION

1.1 Production of Micron Size Engineering Metal Parts

Metal parts, which are used for engineering applications, can be produced by various methods such as forging, stamping, deep drawing, casting and machining [1]. These methods are not suitable especially for hard metals like nickel. In addition, complex geometries and tight tolerances cannot be produced easily with these conventional methods. Electroforming process is more appropriate for production of metal parts which have miniature sizes and complex geometries. This method can be defined as "ionic fabrication", because it provides atomic level controllability, extreme reliability and precision [1, 2].

Electroforming process is defined as "the production or reproduction of an article by electrodeposition upon a mandrel or mould that is subsequently separated from deposit" by The American Electroplaters' and Surface Finishers' Society (AESF) [2]. Electroforming process has mainly three steps:

- Machining: Appropriate material is selected and machined according to the desired geometry. This base material is called as mandrel and its material depends on removing process. It can be soluble chemically or removable physically. Material of the mandrel might be non-conductive or conductive, which totally depends on geometry and cost. The product of the machining step is used as the cathode in an electroplating cell.
- Electroplating: Most important step of the electroforming is electroplating. There are three main components of the electroplating cell; anode, cathode and electrolyte. Mechanical properties of electroformed material are mainly specified by electrolyte type and electrodeposition parameters. Electrolyte is generally used in a liquid form and selected according to electroforming material and desired mechanical properties.

On the other hand, electroplating parameters should be adjusted to obtain most proper mechanical properties and dimensional accuracy.

- Removing/dissolving Mandrel: After electroplating process, mandrel should be removed or dissolved to get the final form of electroformed material. This step should not cause any damage on the final product [3].

Electroforming process has various application areas from thin foils (printed circuit boards, resistive heating tapes, bursting disc, solar panels etc.) to huge parts for aerospace/aircraft industry (moulds, rocket thrust chamber, erosion/corrosion shield) [1, 2]. For example; rotary printing screens, which are used to produce carpets, wallpapers and textiles, are produced by electroforming method. By using electroforming method, any detail can be formed, so electroform method has been mostly preferred to produce moulds. As a matter of fact, electroforming is the only option to form some low tolerances patterns and geometries. Thanks to high resistance against high pressure and corrosion, nickel moulds can be used in injection, compression and resin transfer moulding (RTM) of polymers and additionally, they are used in rubber, glass and powder metallurgy industries. Automotive and aerospace industries often need larger scale moulds. For example; body fairings, radomes, huge engine housings and wing skins. Figure 1 shows the wing skin of a jet, which is produced by electroforming method and has nearly 5 mm thickness and 8.5 m length
[4].

The production of such a huge component, needs high level process control. Otherwise, high amount of nickel and energy are wasted. For this reason, parameters and mandrel selection should be the most suitable for process and product type. As it has been mentioned before, mandrel can be removed physically and reutilized or solved by chemical. In large scale applications, mandrel is mostly removed physically because of cost. If unexpected compression stress occurs, it can damage the mandrel during removal of electroformed part from the mandrel or if there is excess internal stress, electroform can separate from the mandrel at an unexpected time. Both cause time and material wastes. Therefore, electrodeposition parameters are crucial for especially industrial application. Each step of production and process has various necessities.



Figure 1 Nickel mould for wing skins of Harrier. Reproduced from [4].

1.2 The Purpose of the Thesis

Electroforming process is generally used to form engineering metal parts whose geometries are non-uniform and have low tolerances. The production of these parts is a big challenge and for each different geometry; current parameters, electrolyte components and system design should be optimized and adjusted to get the best result.

Metal bellows are elastic vessels which have an accordion geometry. Some examples of different bellow shapes used for certain applications are shown in Figure 2. Bellows can be compressed or extended under pressure. Therefore, they are usually used to sense very small changes in pressure and/or temperature when the inside is filled in with a gas and sealed. Bellows should be flexible, rugged and lightweight and they can be at any size. It has some prominences and recesses which cause nonuniform current distribution. The main purpose of this thesis is the optimization of current parameters to obtain a uniform, flexible bellow having enhanced mechanical properties.



Figure 2 Different bellow shapes Reproduced from [5].

CHAPTER 2

LITERATURE REVIEW

2.1 Fundamental Concepts of Electrodeposition

Electrodeposition basically can be defined as the formation of a metallic film (M) onto a cathodic material by electrochemical reduction of dissolved metal ions (M^{z+}) [6]. This process includes two electrodes and a suitable electrolyte which contains cations (M^{z+}) and anions (A^{z-}) and can be a metallic salt e.g., salt MA [7]. When electric field is applied, cations move to the cathode material. These ions are reduced to metal atoms which initiate buildup of metal electrodeposition layers at micron level [4]. Thanks to this property, metal parts can be produced with low tolerances. Figure 3 shows the electrodeposition process in which current is applied via a power source. The cathode, which is the coated material, is connected to the negative terminal of the power supply and the anode material is connected to the positive one [6].

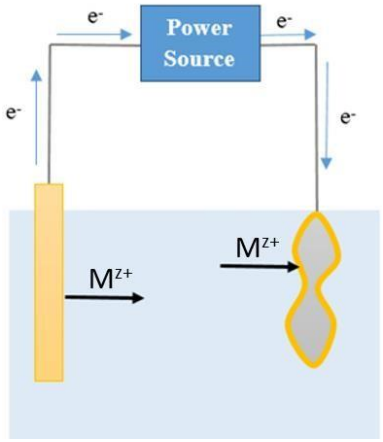


Figure 3 A schematic representation of electrodeposition cell.

The geometrical structure and size of electroformed metal depend on shape of mandrel. The desired thickness in electrodeposition can be obtained by Faraday's Law which is shown in Eq.1. Faraday's law says that the weight of the electrodeposition is directly proportional to the amount of electrical charge which is applied [7].

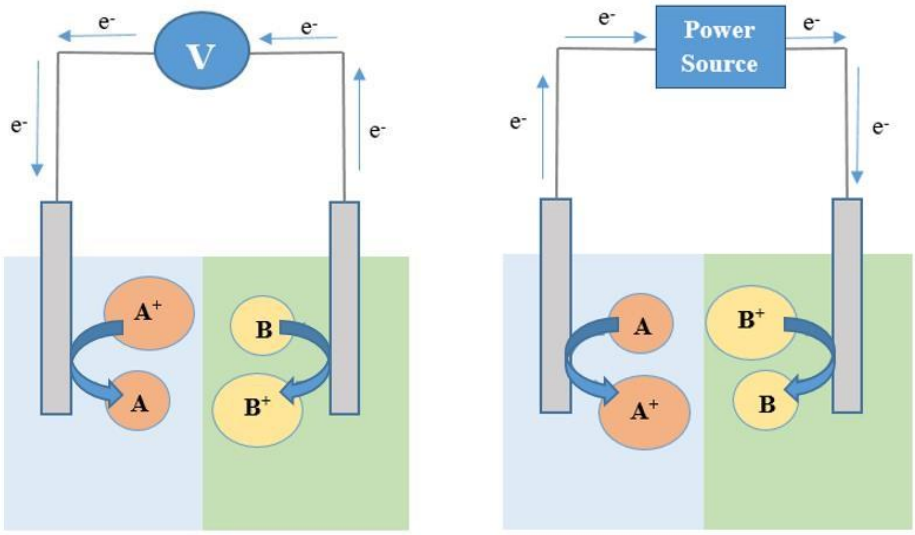
$$W = \frac{M\ I\ t}{z\ F}\eta \qquad (1)$$

where W is the weight of electrodeposition per unit area (g/dm^2), M is molecular weight of depositing material (58.69 g, in the case of nickel), I is the average current density (A/dm^2), t is the time of the experiment (s), z is number of electrons (2, in the case of nickel) and F is Faraday's constant (96485.3329 coulombs/mole e$^-$) and η is the current efficiency of the process. It can be calculated from Eq.2 [8]:

$$\eta = \frac{actual\ weight\ of\ electrodeposition}{theoretical\ weight\ of\ electrodeposition} \times 100 \qquad (2)$$

2.2 Cell Types of the Electrochemistry

There are two types of cells; galvanic and electrolytic. In the galvanic cell (Figure 4.a), chemical energy is converted to electrical energy. Redox reactions occur spontaneously, because Gibbs free energy change of the total reaction is a negative value. In the electrolytic cell (Figure 4.b), electrical energy provides required energy for redox reactions. To initiate and continue the reactions, external energy is used, so redox reactions occur non-spontaneously. Electroplating process is a typical electrolytic cell [9].



(a) (b)

Figure 4 Cell types (a) Galvanic and (b) Electrolytic cells.

Electrode is a conductor which is used to carry electricity from a source to the cell. If oxidation reaction occurs, the electrode is called as anode otherwise, reduction reaction occurs, it is called as cathode [6]. M^{z+} ions move from electrolyte to cathode surface, then they enter into crystal lattice. This procedure provides excess amount of electrons on the metal and it becomes negatively charged, q_M^-. This negative charge attracts positive metal ions (M^{z+}). Higher amount of M^{z+} ions in solution at around the cathode causes slower movement of ions from crystal lattice to solution compared to movement from solution to crystal structure. Eq.3 shows the equlibrium between metal and metal ions:

$$M^{z+} + ze^- \rightleftarrows M \quad (3)$$

where z is the number of electrons. The reaction from left to right shows reduction reaction and reverse direction indicates oxidation reaction [7]. These reactions occur non-spontaneously in an electrolytic cell. Eq.4 is used to calculate required minimum energy to initiate reaction:

$$\Delta G = -zFE^o_{cell} \quad (4)$$

where z is valence electron, F is Faraday's constant and E^0_{cell} is the reversible cell potential. The differences between cathode and anode reduction potentials gives reversible potential of an electrolytic cell (E^0_{cell}). Standard electrode potential of an electrode is calculated at 25°C. The practical cell potential can be obtained from Nernst equation given in Eq.5. This equation shows that electrode potential is related to activity of ions:

$$E_{eq} = E^o + \frac{RT}{zF} \ln \frac{\Pi\alpha(ox)}{\Pi\alpha(red)} \quad (5)$$

where α is activity of metal ion (M^{z+}) in solution, R is gas constant (8.31 J/ mole K) and T is absolute temperature (K). Actual cell potential shifts from equilibrium potential value according to polarization type. This shifting is called as an overpotential (η) and it is shown in Eq.6:

$$\eta = |E - E_{eq}| \tag{6}$$

It can be anodic (η_A) or cathodic (η_C) overpotential depending on direction of reaction [10]. There are three reaction mechanisms which provide ion transfer to surface of the electrode i) migration (potential gradient as a driving force), ii) diffusion (concentration gradient as a driving force), iii) convection. If the reaction rate depends on surface reaction, the overpotential necessary to overcome activation energy barrier is called as activation overpotential (η_{Act}) [6,10]. In an electrochemical process, two types of current can be generated; anodic (I_A) and cathodic (I_C), which are positive and negative, respectively. In equilibrium, anodic and cathodic currents are equal to each other and there is no net current. This is represented in Eq.7:

$$|I_A| = |I_C| = i^o \tag{7}$$

where i^o is exchange current density which shows the rate of redox reactions in equilibrium. When the system is connected to any electron source, the equilibrium is disturbed and the number of electrons which flow into metal increase. The metal is charged negatively and it attracts more cations. This electrode becomes cathode and the other electrode becomes anode. Anodic and cathodic currents can be represented as:

(8) $$i_A = i^o e^{\frac{\alpha * F * z}{R * T} * \eta Act}$$

(9) $$i_C = -i^o e^{-\frac{(1-\alpha) * F * z}{R * T} * \eta_{Act}}$$

where α denotes transfer coefficient, which is in the $0< \alpha <1$ range. R is gas constant

(8.3145 J/mol K) and T is absolute temperature [10]. For 25°C, these equations can be rewritten as:

$$f = \frac{F}{RT} \tag{10}$$

$$f = \frac{96487\ C\ mole^{-1}}{8.3145\ J\ mole^{-1}\ K^{-1}\ 298\ K} = 38.94\ C \times J = 38.94\ V \tag{11}$$

If the logarithms of Eq.8 and Eq.9 are taken and solved for η, Tafel equation (Eq.12) can be obtained:

$$\eta = a \pm b \log |i| \tag{12}$$

$$a = \frac{2.303RT}{\alpha zF} \log i^{o} \tag{13}$$

$$\mathrm{b} = \frac{2.303\ \mathrm{R\ T}}{\alpha\ \mathrm{z\ F}} \tag{14}$$

in Tafel equation (Eq.12), a and b are constants. i^{o} is exchange current density and i is current density [7, 11]. Tafel equation express relationship between overpotential and faradaic current [12]. This relation is applicable for high overpotential systems and in the absence of mass transfer effect on the current. The idealized Tafel plot is shown in Figure 5. The slope of the linear region gives anodic and cathodic transfer coefficients and open circuit potential (OCP) [13], which is the experimental voltage value at zero current [14] and it can be found from Tafel plot.

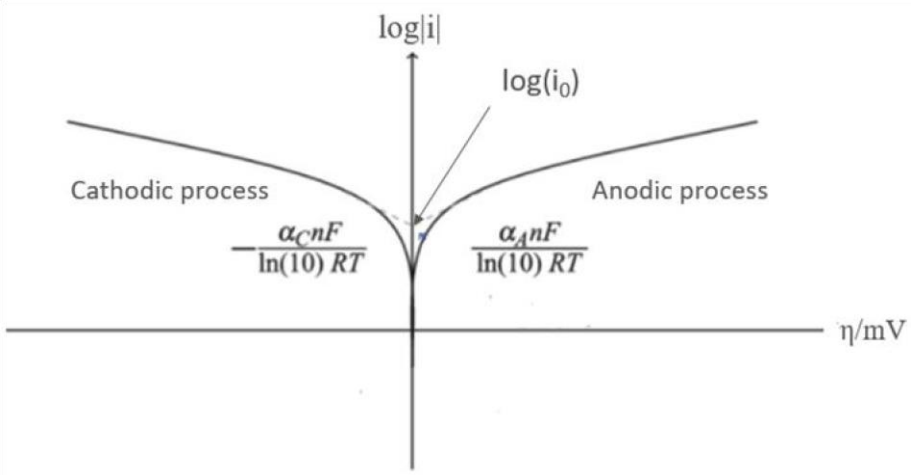


Figure 5 Idealized Tafel Plot [13].

On the other hand, reaction rate can be limited by diffusion, which is called as concentration polarization (η_{Con}) that is caused by the concentration differences between electrode surface (catholyte) and the bulk solution [6,10]. These terms become more understandable after Butler-Volmer equation is learned with details. When interface deviates from equilibrium, net current density is determined by Butler-Volmer equation. Figure 6 shows interphase for equilibrium and deviation from equilibrium situations [15]. In equilibrium point, anodic and cathodic currents are equal to each other, it is also called as exchange current density. The deviation from equilibrium is expressed with η, which can have a positive or a negative value.

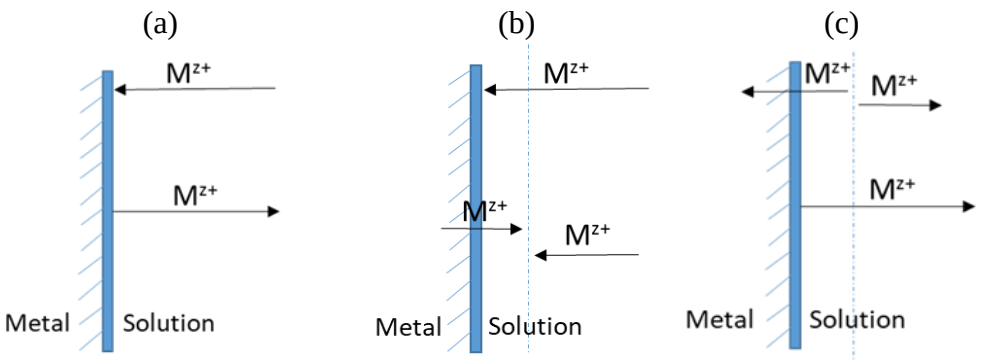


Figure 6 Cathode-electrolyte interface a) equilibrium, b) and c) deviations from equilibrium [15].

Butler-Volmer equation is used to predict overall current (Eq.15) as a function of overpotential:

$$i = i_C - i_A \tag{15}$$

Both currents can be written as:

$$i_C = \alpha\ F\ k_f C_o(0,t) \tag{16}$$

$$i_A = \alpha\ F\ k_b C_o(0,t) \tag{17}$$

where F is Faraday constant, A (cm^2) is area of the electrode and C_j (x,t) (mol cm^{-3}) is the concentration of species j at the distance x (cm) from the electrode at the time t (s).

k_f and k_b can be written as a function of the standart heterogeneous rate constant k^o:

$$k_f = k^o e^{-\alpha\, f\, (E-E^o)} \tag{18}$$

$$k_b = k^o e^{(1-\alpha) f\, (E-E^o)} \tag{19}$$

Eq.15 can be rewritten as:

$$i = F\ \alpha\ k^o [C_o(0,t) e^{-\alpha\, f\, (E-E^o)} - C_R(0,t) e^{(1-\alpha) f\, (E-E^o)}] \tag{20}$$

Eq.20 is one of the fundamental equations of electrochemistry called as ButlerVolmer equation. This equation can be applicable for prediction current of electrochemical reaction as a function of overpotential [16] in other words it gives

dependency of overpotential on current density [12]. When current density is high, dissolution rate of metal ions is not as fast as deposition rate [7]. In this situation, catholyte has lower metal ion concentration than the bulk of the electrolyte. The concentration differences between catholyte and bulk solution causes concentration polarization [10].

2.3 Nickel Electrodeposition

Nickel electrodeposition is one of the most frequently used surface treatments and also nickel is preferred for electroforming applications. Electrodeposited nickel provides some enchanced mechanical properties such as high erosion and corrosion resistance, low internal stress and high hardness [17]. Thanks to these mechanical properties, nickel is frequently preferred for engineering applications. Electrodeposition process basically requires two electrodes (anode and cathode) immersed in an electrolyte which provides ionic conductivity. In nickel electrodeposition, nickel is used as a soluble anode and cathode could be any material with sufficient electrical conductivity [18]. Properties of the electrodeposit depend on bath type and working conditions such as pH, temperature and agitation. However, there are several bath types in literature. Among them, mostly Watts and sulphamate baths are used. Watts bath is the major bath type for decorative electroplating applications, because of low cost and easy inspectability [19]. On the other hand, in engineering processes and electroforming, sulphamate bath is mostly preferred, because it provides coatings having the lowest internal stress, highest ductility, highest deposition rate and highest purity of all nickel bath types [20]. Internal stress of the Watts and sulphamate baths are compared in Figure 7 [21]. Lower internal stress is essential for electroforming applications because high compressive or tensile stress can cause; i) difficulty and distortion during separation of electroform from , ii) peeling, folding or separation of electroform from mandrel before the desired thickness is achieved, iii) flexion and blistering of electrodeposition [22].

In addition, nickel sulphamate bath has superior throwing power which is useful for plating complicated geometries [19]. Throwing power can be described as the ability

to deposit uniformly on complex geometries [23]. It generally depends on operating conditions (temperature, pH, current density and agitation) and electrolyte composition [24]. Recessed and prominent areas can be equally deposited with high throwing power [7]. Its effect is shown in Figure 8. Sharp edges receive higher voltages and become thicker than recessed areas.

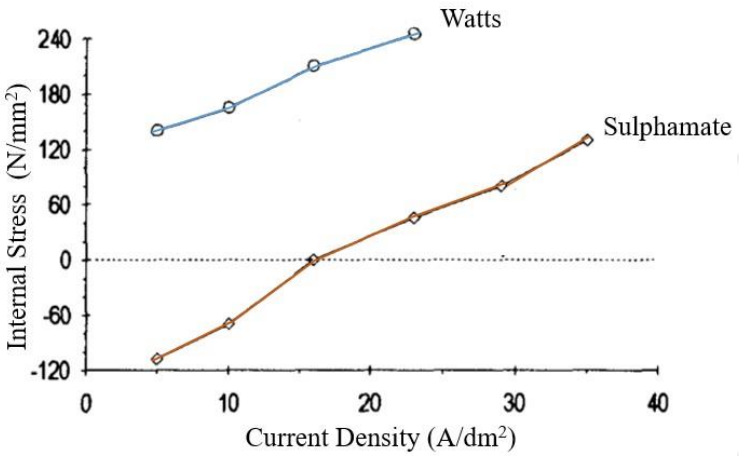


Figure 7 Comparison of internal stress of nickel coatings on bath type and current density [21].

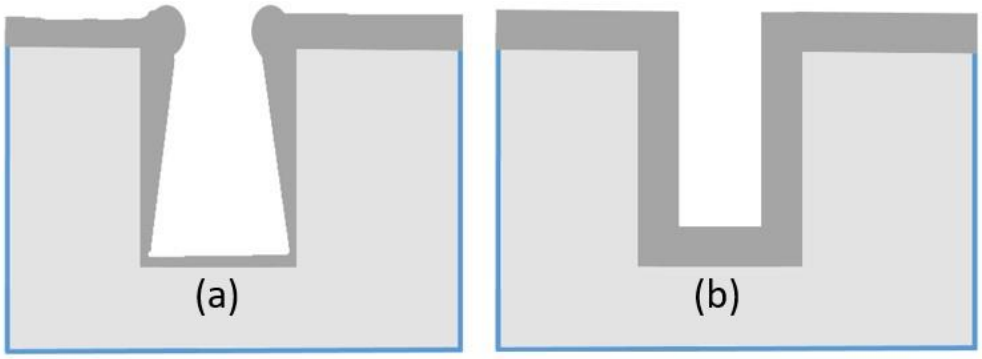


Figure 8 Effects of throwing power a) low b) high throwing power

Table 1 shows chemical compositions and operating conditions of nickel sulphamate bath. Nickel sulphamate is the main source of nickel ions and it should have very high purity. Boric acid acts as a buffer solution which is used for stabilizing pH of the

solution in the range during the operation [19]. Although it causes some internal stress in the deposit, a small amount of nickel chloride is added into sulphamate bath to prevent anode passivation and increase throwing power. Rama char et al. [25,26] claimed that an anode efficiency of 60-80% was obtained without nickel chloride. On the other hand, when 20 g/l nickel chloride is added to bath, anode efficiency becomes almost 100%.

Mechanical properties of the electrodeposit mainly depends on bath composition and operating conditions. To obtain the optimum mechanical properties for a certain application, operating conditions and chemical composition should be adjusted. There are some common difficulties in maintaining nickel electrodeposition baths which will be discussed in the following sections.

2.3.1 Anode Passivation

Under normal operating conditions, anode has almost 100% efficiency. When pH becomes too high, hydroxyl ions discharge and inhibit dissolution of nickel [19]. Another passivation process is shown in Eq.21 where passivating coverage of hydroxylated nickel precipitate [18].

$$Ni^{+2} + 2OH^{-} \rightarrow Ni(OH)_2 \qquad (21)$$

Table 1 Bath contents and working conditions of sulphamate bath [19].

Temperature (°C)	32-60
pH	3.5-5
Agitation	Air or mechanical
Current Density (A/dm^2)	0.5-30

Nickel Sulphamate (g/l)	300-450
Boric Acid (g/l)	30-45

2.3.2 Hydrogen Evolution

Small amount of hyrdogen discharge is generated at the cathode surface (Eq.22). during nickel plating. Hydrogen evolution is one of the most important problem against high quality electrodeposition, because hydrogen bubbles cause pittings on the cathode surface. The cathode efficiency drops to 97-92% because of this side reaction [19].

$$2H^{+}(l) \rightarrow H_2(g) \qquad (22)$$

Furthermore, hydrogen evolution causes high internal stress which is another important drawback for especially electroforming applications [27]. Another result of the excess hydrogen absorption is hydrogen embrittlement. Hydrogen atoms are much smaller than nickel atoms, so they can migrate to crystal lattice of the nickel and then weaken the atomic bonding. This situation causes loss of ductility and ease of crack initiation [28].

2.3.3 pH Changes

Although nickel sulphamate bath has high stability under normal conditions, utilization of sulfamic acid causes more hydrolysis. Eq. 23 shows hydrolysis reaction of the nickel sulphamate:

$$NH_2SO_3^{-} + H_2O\ (l) \rightarrow NH_4^{+} + SO_4^{2-} \qquad (23)$$

As a result of this reaction, ammonium ion (NH_4^{+}) is generated. At the same time, pH of the solution increases because of NH_4^{+} generation [18]. Besides hydrolysis reaction, hydrogen evolution reaction increases the pH. Under normal circumstances, the pH of the nickel sulphamate bath tends to increase and it can be

decreased by adding sulfamic acid. Sometimes pH can drop unexpectedly due to anode passivation [29].

2.3.4 Non-Equal Current Distribution

Especially for low-tolerance geometries, current distribution is a very important factor. The thickness at any point is directly related to current density at that point. Some factors, such as distance of the part relative to anode and its geometry affect current density distribution. Figure 9 shows that prominent parts of the cathode has higher current density, so these parts become thicker than other parts of cathode [29]. On the other hand, because the distance between recessed regions and anode is longer, these regions have higher resistance to current flow [7]. Anode is other factor for uniform electrodeposition. It should have a uniform structure to provide homogenous current density. As it is shown in Figure 9, when non-uniform anode shape is used, current is distributed non-homogeneously [29].

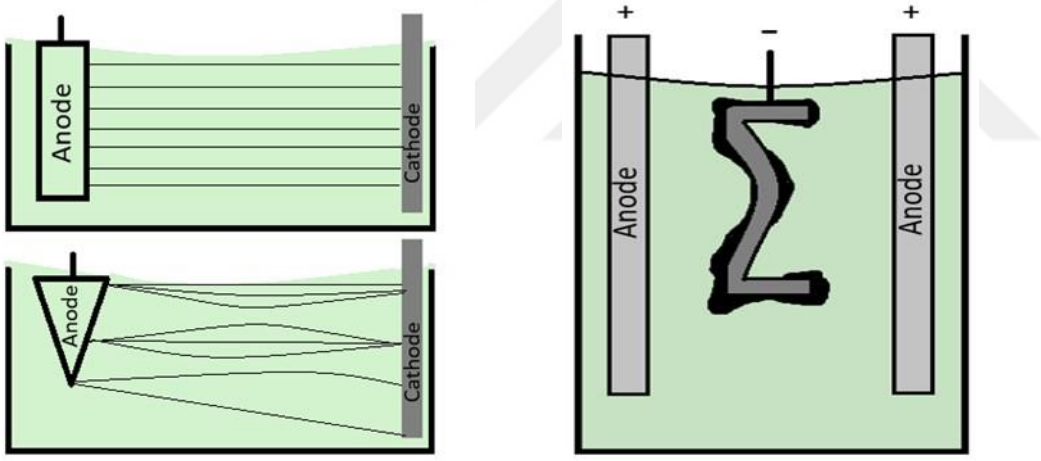


Figure 9 Examples of non-uniform current distributions in electroplating [29].

To prevent non-equal thickness distribution, some non-conductive materials can be tailored according to geometry and they act as a shield to block excess current on the prominent areas. Additionally, anode should be appropriate for cathode size and geometry. For example; when cylindrical cathode is used, an anode must be adjusted so that each surface can be seen [7]. For some geometry which are very complex and

small size, shields cannot be used. For this reason, different current types are applied for these geometries instead of direct current. Pulse-reverse current method is very useful for low tolerance micron size electroforming applications [30].

2.4 Pulse-Reverse Current Method

Enhanced mechanical properties can be obtained by pulse reverse current method [31]. It is known that grain size significantly affects mechanical properties of crystalline metal deposits. When pulse-reverse current is applied, smaller grain size is obtained compared to direct current method [32]. As a result of finer grain size, better mechanical properties are attained. This method is also used for complex geometries because it provides more homogenous electrodeposition thickness.

2.4.1 Working principle of the Pulse reverse method

In pulse-reverse method (PRC), voltage or current is alternated between two values which are called anodic and cathodic voltage/current. Despite the fact that there are a lot of pulse-reverse wave forms, only one type (bipolar wave form) was investigated within the scope of present study. Cathodic current, as shown in Figure 10, (I_{CC}) has a positive value and provides dissolution of anode and coating onto cathode. On the other hand, when negative voltage is applied (anodic current (I_{AA})), cathode is partly dissolved into electrolyte. Excess part of the electrodeposition is diminished thanks to this procedure which also provides high ion concentration in the electrolyte and high nucleation rate.

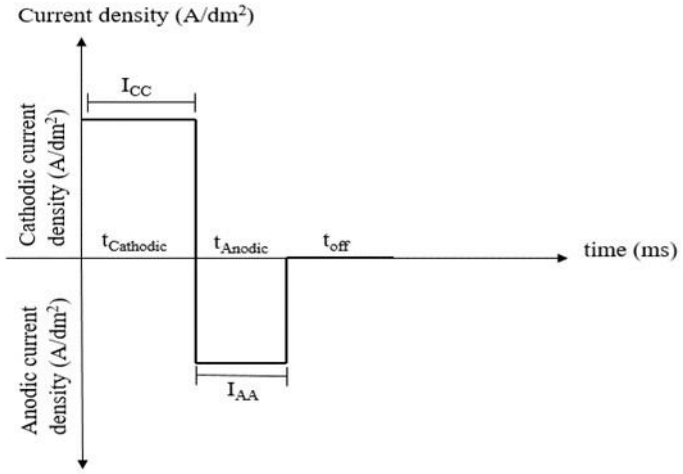


Figure 10 Pulse-reverse bipolar current wave shape [33].

Mechanical properties of nickel electroforms can be improved by adjusting current parameters and components of solution. Researchers have mostly used traditional direct current method (DC) to get the desired mechanical properties. However, there is only one parameter which is called current density (A/dm^2) in DC method. Pulse reverse current method (PRC) have four independent parameters; anodic time (t_A), cathodic time (t_C), anodic current (I_A) and cathodic current (I_C). In addition to these independent parameters; duty cycle, frequency and average current density can be adjusted to obtain enchanced mechanical properties. These are calculated as:

$$I_{av} = \frac{(I_{CC} x t_{Cathodic}) - (I_{AA} x t_{Anodic})}{t_{Cathodic} + t_{Anodic} + t_{off}} \quad (24)$$

$$frequency = \frac{1}{t_{Cathodic} + t_{Anodic} + t_{off}} \quad (25)$$

$$duty\ cycle = \frac{t_{Cathodic}}{t_{Cathodic} + t_{Anodic} + t_{off}} \quad (26)$$

When direct current is applied, dissolved ions are deposited onto mandrel and ion concentration becomes stable. In pulse current method (PC), anode is dissolved and then zero current is applied. Nondeposited ions are accumulated in electrolyte and ion

concentration becomes higher during t_{off} (See Figure 11) [34]. When PRC method is used as the current type, reverse current dissolves part of the plating at the cathode into the electrolyte, which provides even higher ion concentration than PC method

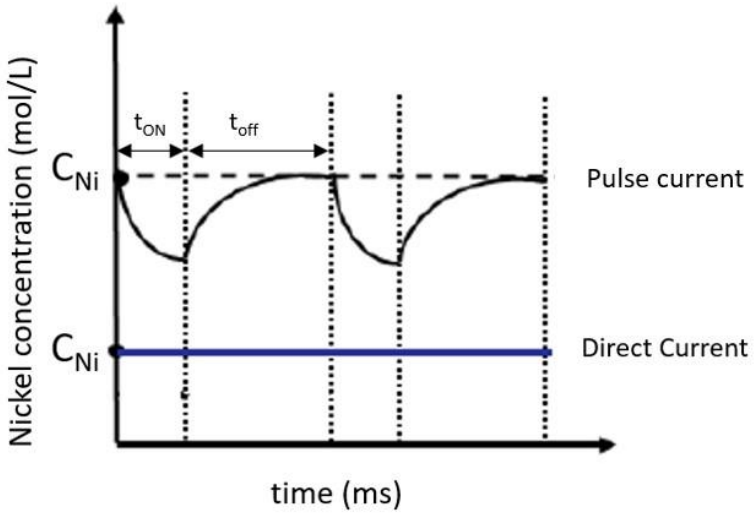


Figure 11 The change of concentration with time in DC and PC [34].

2.4.2 Effect on Microstructure

In PRC, nucleation rate is higher than DC because of higher ion concentration and higher voltages applied during pulse current which provides finer grain size compared to direct current method. There are many parameters which can be adjusted to obtain finer grain size. According to Tafel equation, the larger current density causes larger overpotential [35]. Following the electro crystallization theory, the activation energy of nucleation becomes lower, when higher cathodic overpotential is applied and as a result, nucleation rate increases [31]. High nucleation rate ensures finer grain size. Grain size reduction can also be obtained by additives which are mainly used in large scale production. Although using additives ensures better surface without any special treatment, it significantly increases internal stress [21].

Chapparro et. al. [36] compared three methods: direct current, pulse current and pulsereverse current. Their study revealed the change of microstructure with current type. More uniform thickness distribution, smoother surface and finer grain size could

be obtained by applying PRC method [36]. In another study which investigated the effect of current parameters on microstructure in PC, Xuetao and his colleges found that when $t_{cathodic}$ increased from 0.1 to 3 ms, grains became finer. But if $t_{cathodic}$ was higher than 8 ms, again coarser grains were formed. In the same study, the effects of t_{off} was also studied. It was observed that increasing the t_{off} from 5 to 20 ms, lead to coarser grain sizes [35].

2.4.3 Effect on Mechanical Properties

Internal stress is a crucial property for electroforming process. The study of Yeh et. al. [37] demonstrated that PRC method provided lower internal stress compared to DC method. In the same study, the effect of current density on internal stress was also investigated. Although, applying high current density reduces the time and energy consumption, it has some negative effects in electrodeposition process. When a high current density is applied in DC method, anode is dissolved and dissolved ions are deposited continuously. Therefore, there is not enough time for diffusion. Since the rate of reducing ions determines the internal stress, internal stress is increased with current density which is definitely not desired.

In the PRC mode, high cathodic current density avoids absorption of hydrogen species into cathode and the reverse current and off time allows time for diffusion. Thus, electrodeposition has lower internal stress and lower roughness compared to DC method at a high current density [37].

According to grain boundary strengthening mechanism, grain boundaries help to block dislocation motion, which means more grain boundaries provide strengthened microstructure. Since hardness is the resistance to plastic deformation which depends on the dislocation motion, as the electrodeposits have finer grain, the hardness of them increases accordingly [31]. Effects of peak current density on microstructure and mechanical properties are investigated by Shao and his colleagues [31]. They observed that hardness increased with current density [38]. This result can be an evidence for grain boundary strengthening mechanism. In another study performed to enhance mechanical properties of the nickel electrodeposition, Park et al. [39] investigated the effect of PRC parameters on hardness and friction coefficient. Two different average

current densities were used to show the effects of frequency on hardness and friction coefficient. There was an inverse correlation between hardness and friction coefficient. When the frequency was increased, friction coefficient decreased and hardness increased for both average current density values. This study also showed that lower average current densities provide better mechanical properties such as high hardness and low friction coefficient [39].

CHAPTER 3

EXPERIMENTAL PROCEDURE

Aluminum mandrels which had accordion geometry or copper coupons were used as the cathode materials in the following experiments. Because of their different structures and materials, different experimental procedures were applied. All parameters were optimized by using coupon based experiments and optimized parameters were used to electroform the accordion geometry.

Process and characterization equipments of the study are summarized as:

- Power supply for pulse plating: Pulse pe86CB 3HE (maximum voltage 25, maximum DC current 5 A, pulse current 25 A)
- Power supply for DC plating: Agilent B2901A Precision Source
- Hot Plate: MTOPS HD180 Hot plate & Magnetic stirrer
- pH Meter: Thermo Scientific Orion Star A111 pH Benchtop Meter Kit Rotating motor: Optimum D 250x550 Power Lathe
- Pump for electrolyte circulation: Jebo External 829 Bio-chemical Filter
- Scaning Electron Microscope (SEM): FEI Nova NanoSEM 430
- X-RayDiffraction Analysis (XRD):Rigaku DMAX 2200 X-ray
  Diffractometer equipped with a 3kW power generator (working at 40 mA and 40 kV, Cu Kα was used as X-Ray sources, scan rate is selected 2^{o}/min)
- Micro hardness measurement: Shimadzu HMV- G21 Micro Vickers Hardness Tester
- Tensile test device: Instron 5565A Load Frame
- Heat treatment furnace: Mikrotek MFX 1005 Furnace
- Digital Microscope: Nikon ShuttlePix P-MFSC

The list of chemicals which were used in present study are:

- Nickel Sulphamate ($Ni(SO_3NH_2)_2\ 6H_2O$): 63035981 Umicore, Belgium
- Nickel Chloride ($NiCl_2$): 339350 Sigma Aldrich
- Boric Acid (H_3BO_3): 1001659012 Merck
- Copper Pyrophosphate Trihydrate ($Cu_2P_2O_7.3H_2O$): 344699 Sigma Aldrich
- Potassium Pyrophosphate ($K_4P_2O_7$): Sigma Aldrich
- Potassium Nitrate (KNO_3): 221295 Sigma Aldrich
- Ammonium Hydroxide Solution (NH_4OH): 105428 Merck
- Hydrochloric Acid (HCl): 100317 Merck
- Hydrofluorıc Acid (HF): 30103 Sigma Aldrich
- Nitric Acid (HNO_3): 100452 Merck
- Sodium Hyroxide (NaOH): 106469 Merck
- Zinc Oxide (ZnO): 108849 Merck

3.1. Coupon Based Experiments

Copper coupon cathodes and nickel anodes were used in nickel sulphamate based electrolyte to determine process conditions during electroforming. In the determination of the thickness of the electrodeposition, the required thickness for hardness measurements was considered. At least 30-40 micron thickness electrodeposition is needed for reliable hardness measurements. For this reason, the thickness of the coupon based experiments was taken as 40 microns. The steps that are followed during coupon based experiments are given below:

3.1.1. Pretreatments

Surfaces of electrodes should be clean and active for reactions. Passivated anode and cathode cause a decrease in efficiency and quality of the electrodeposition [19]. If the surface of the cathode is not cleaned properly, atoms cannot be adsorbed onto the electrode. Likewise, when nickel anodes are not activated, they cannot be dissolved adequately. Because of these reasons, pretreatments have crucial importance in electrodeposition process. The pretreatment processes for the cathode applied in this study are given in Figure 12. Firstly, copper was masked with a special

electrochemistry tape (3M Electroplating Tape 470) which has resistance to chemicals used in plating and pretreatment processes Masking was used for demarcation of the plating area. After masking, the copper coupon was immersed in a 0.5 M sodium hydroxide solution (NaOH) for 1 minute. This process helped removal of grease and soil and then the cleaned copper was immersed in a 50 v/v % nitric acid (HNO_3) solution (balance water) where the oxide layer of the copper surface was dissolved. Cathode was washed with distilled water before and after all the steps.

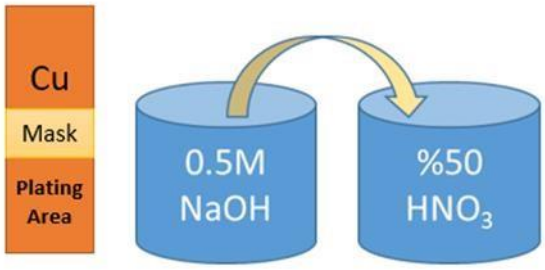


Figure 12 Schematic drawing of a copper coupon and the pretreatment process for cathode.

Next step was the preparation of nickel anode. Anode was chosen according to the cathode area and shape. In this part of the experiments, rectangular shape anode was used and anode area was adjusted to be the twice of the cathode area. Anode was activated by 25 v/v % hydrochloric acid (HCl) solution (balance water).

3.1.2. Preparation of the Electrolyte

Nickel sulphamate bath was chosen for this research. The bath composition was not studied in this work, so conditions and composition of the electrolyte were selected according to the literature review [40,41]. Table 2 includes operation conditions and solution composition for nickel sulphamate bath. Temperature was controlled by a hot plate with a contact thermometer and pH was measured. If the pH was higher than 4.5, sulfamic acid was added to adjust it.

Table 2 Operating conditions and composition of nickel sulphamate bath.

Temperature (°C)	50
pH	4.5
Agitation	Mechanical
Nickel Sulphamate (g/l)	350
Boric Acid (g/l)	30
Nickel Chloride (g/l)	12

3.1.3. Cell Design and Electrodeposition

After all pretreatments were completed, electrodes were immersed into an appropriate size beaker. The cell was placed on a hot plate, which had magnetic stirrer and provided the required heat to reach 50 °C. A photograph of the cell is demonstrated in Figure 13. The distance between anode and cathode was fixed at 10 cm. Anode was connected to the positive terminal of the power supply and cathode was connected to the negative one. Solution was agitated with the help of the magnetic stirrer which provided homogenous temperature and composition distribution.

Coupon based experiments were performed to optimize the anodic to cathodic current ratio together with average and peak current densities. One parameter was studied at a time. Firstly, average current density was studied. Then the effects of the peak current density and the ratio of pulse current to reverse current on microstructure were investigated. Table 3 summarizes the investigated parameters.

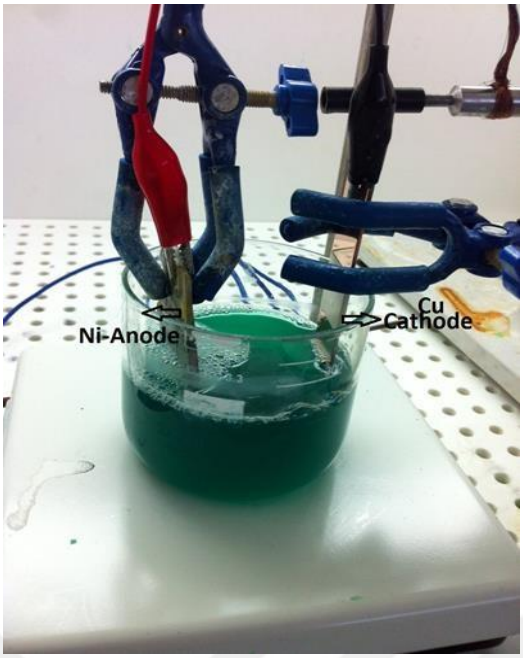


Figure 13 A photograph of the cell used in coupon based experiments.

3.2 Experiments to form Accordion Geometry

Parameters, which were optimized in coupon based experiments, were applied for accordion geometry. Thanks to these experiments, the pulse-reverse current (PRC) effect on homogeneous distribution was investigated. The main purpose of these experiments was to obtain equal thickness distribution between prominent and recessed regions.

3.2.1. Pretreatments

Aluminum was selected as the mandrel material because it can easily be machined and chemically dissolved. Besides advantages of the aluminum, it has a disadvantage for electrodeposition process. It cannot be easily coated with nickel, since it has an oxide layer. Pretreatment of aluminum has attracted great attention due to adhesion problem. One of the pretreatment processes utilize copper coating on aluminum to overcome adhesion problem. Therefore, 10 μm copper was plated onto the mandrel, before nickel was deposited in this study. However, surface of aluminum mandrel was

prepared to accept copper prior to plating. This preparation treatment is demonstrated in Figure 14.

Table 3 The parameters used to study pulse-reverse nickel electrodeposition.

Optimization Parameter	I_{CC} (A/dm^2)	Ratio	I_{AA} (A/dm^2)	$t_{Cathodic}$ (ms)	t_{Anodic} (ms)	t_{off} (ms)	$I_{average}$ (A/dm^2)
Ratio of pulse current to reverse current	20.00	0.10	2.00	0.30	0.10	3.50	1.50
	20.00	0.30	6.00	0.30	0.10	3.20	1.50
	20.00	0.60	12.00	0.30	0.10	2.80	1.50
	20.00	0.90	18.00	0.30	0.10	2.40	1.50
	20.00	1.00	20.00	0.30	0.10	2.30	1.50
	6.00	0.30	20.00	8.00	1.00	10.00	1.50
	12.00	0.60	20.00	4.00	1.00	14.00	1.50
	18.00	0.90	20.00	2.00	1.00	8.00	1.50
Average current density	20.00	1.00	20.00	0.30	0.10	3.60	1.00
	20.00	1.00	20.00	0.30	0.10	1.60	2.00
	20.00	1.00	20.00	0.30	0.10	0.94	3.00
	20.00	1.00	20.00	0.30	0.10	0.60	4.00
	20.00	1.00	20.00	0.30	0.10	0.40	5.00
Peak current density	20.00	1.00	20.00	0.30	0.10	2.25	1.50
	30.00	1.00	30.00	0.30	0.10	3.60	1.50
	40.00	1.00	40.00	0.30	0.10	4.90	1.50
	50.00	1.00	50.00	0.30	0.10	6.25	1.50
	60.00	1.00	60.00	0.30	0.10	7.60	1.50
	70.00	1.00	70.00	0.30	0.10	8.90	1.50
	80.00	1.00	80.00	0.30	0.10	10.20	1.50
	90.00	1.00	90.00	0.30	0.10	11.60	1.50
	100.00	1.00	100.00	0.30	0.10	12.90	1.50
	110.00	1.00	110.00	0.30	0.10	14.20	1.50
	120.00	1.00	120.00	0.30	0.10	15.60	1.50

Firstly, aluminum mandrel was immersed into a 0.5 M sodium hydroxide solution which helped to remove soil and grease. Then oxide layer was removed by first acid solution (%25 v/v hydrofluoric acid, %75 v/v nitric acid). After surface was activated, aluminum mandrel was immersed into a zincate solution (525 g/l NaOH, 100 g/l ZnO) and coated with a thin zinc layer. Thanks to this step, reoxidation of the aluminum was

avoided. Zincated aluminum was immersed into a nitric acid solution to remove weakly adherent zinc atoms and then second zincate treatment was applied [42].

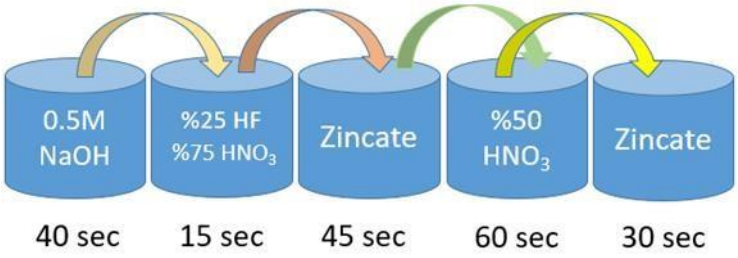


Figure 14 Zincate treatment for aluminum mandrel.

There are many copper plating electrolytes in the literature [19,40]. Among them, copper pyrophosphate strike solution was selected as the plating bath. Strike baths can be used only for thin layer coatings, up to several micrometers of plating. The solution composition is listed in Table 4. Copper plating has strong adherence, when it is plated from pyrophosphate strike bath. Potassium salts have high solubility and conductivity, so pyrophosphate strike electrolyte has a high throwing power. Ammonia helps anode corrosion and pH control. Also it provides brightening to copper deposition. Potassium nitrate avoids reduction of hydrogen so the operation can be done at a higher current density. The pH is one of the most important parameters because when pH decreases, the throwing power of the cell decreases and it is undesirable for plating complex geometries. Another possibility is the high pH which causes lower anode efficiency [43]. In the present study, the selected bath was used at room temperature and a constant voltage was applied (1 V). Tube shaped copper anode was used due to cylindrical cathode geometry. Air agitation was placed at the bottom of the cathode. The oxide layer of the copper anode was removed by %50 nitric acid (HNO_3) before aluminum mandrel was plated with copper by DC.

3.2.2. Cell Design and Electrodeposition

The same nickel sulphamate bath that was used in the coupon based experiments was employed in the electrodeposition of accordion geometry. Agitation was accomplished by the supply of air which also prevented pitting (H_2 bubble) formation. Because of the complex geometry, homogeneous current distribution could not be provided easily. In addition to the PRC method, rotation of cathode was used for equal metal distribution. Experimental setup is shown in Figure 15. An enhanced filtration system was used to avoid any contamination. Rotation rate and flow rate of the electrolyte were fixed at 125 rpm and 0.02 L/s, respectively.

All parameters could not be investigated within the scope of these experiments, due to high cost of the mandrel and complicated system. Therefore, some optimized parameters were selected and applied for accordion geometry in furtherance of homogenous nickel distribution.

Table 5 summarizes the parameters which were studied in this part of the research. These parameters were investigated for homogeneous current distribution for complex geometries.

Table 4 Copper pyrophosphate strike bath composition and operating conditions [43].

Temperature (°C)	22-30
pH	8.0-8.5
Agitation	Air
Current density (mA/cm^2)	10-30
Copper Pyrophosphate Trihydrate (g/l)	350
Potassium Pyrophosphate (g/l)	112-205
Potassium Nitrate (g/l)	1.5-3.0
Ammonium hydroxide (ml/l)	0.5-1.0

Table 5 Studied parameters for accordion geometry.

I_{CC} (A/dm^2)	Ratio	I_{AA} (A/dm^2)	$t_{Cathodic}$ (ms)	t_{Anodic} (ms)	t_{off} (ms)	$I_{average}$ (A/dm^2)
20.00	0.10	2.00	0.30	0.10	3.50	1.50
20.00	0.50	10.00	0.30	0.10	2.80	1.50
20.00	1.00	20.00	0.30	0.10	2.30	1.50

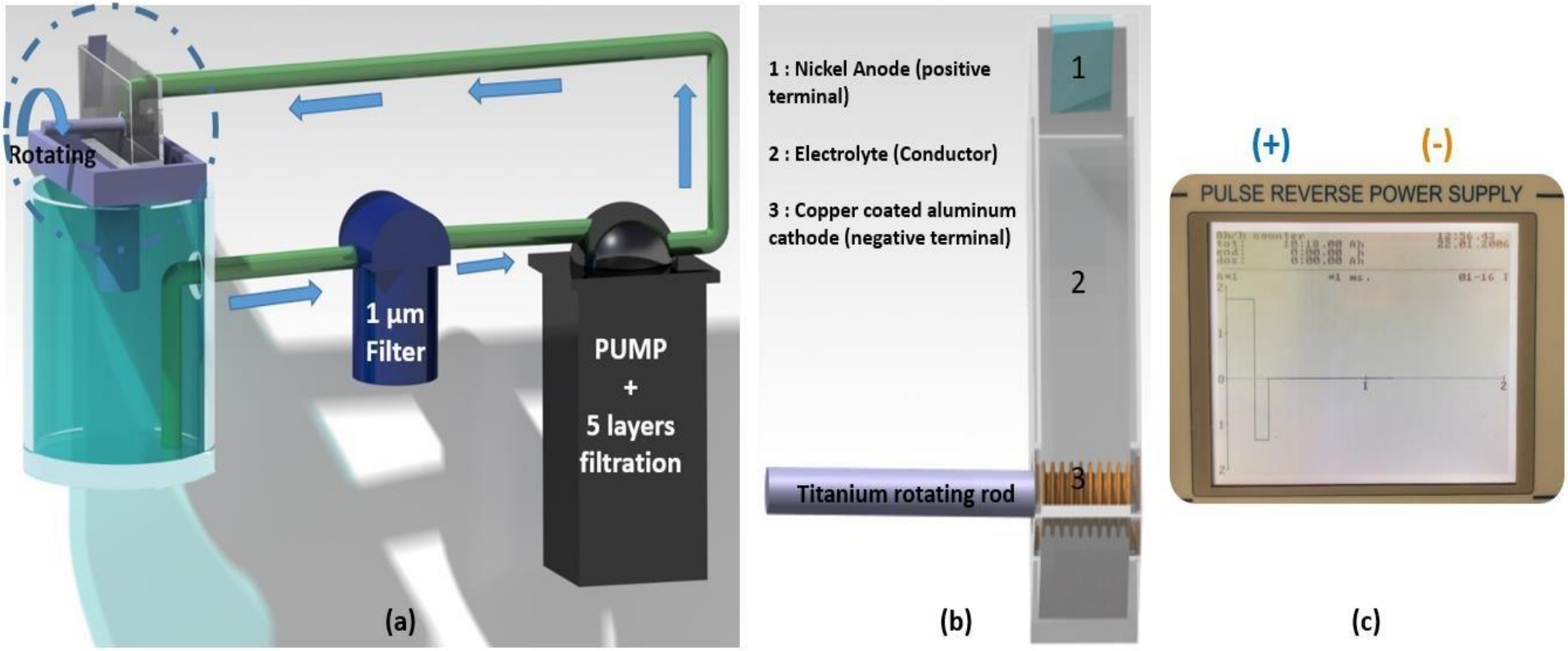


Figure 15 (a) A schematic of experimental set-up for plating accordion geometry (b) Electroplating cell and (c) The secreen of power supply.

CHAPTER 4

RESULTS AND DISCUSSION

4.1 Application of DC, PC and PRC Methods

Electroforming of bellow geometry using DC method was simulated through COMSOL Multiphysics® 5.2 software. The simulation of electrodeposition is shown in Figure 16. The color difference represents the thickness distribution. As it was expected, the prominence regions of mandrel were thicker than recessed areas. It should be followed that, it is directly related with voltage distribution and anodecathode distance. Outer thickness was 9 times thicker than inner thickness. These results confirmed the necessity of using different techniques to obtain homogeneous deposition on the accordion geometry.

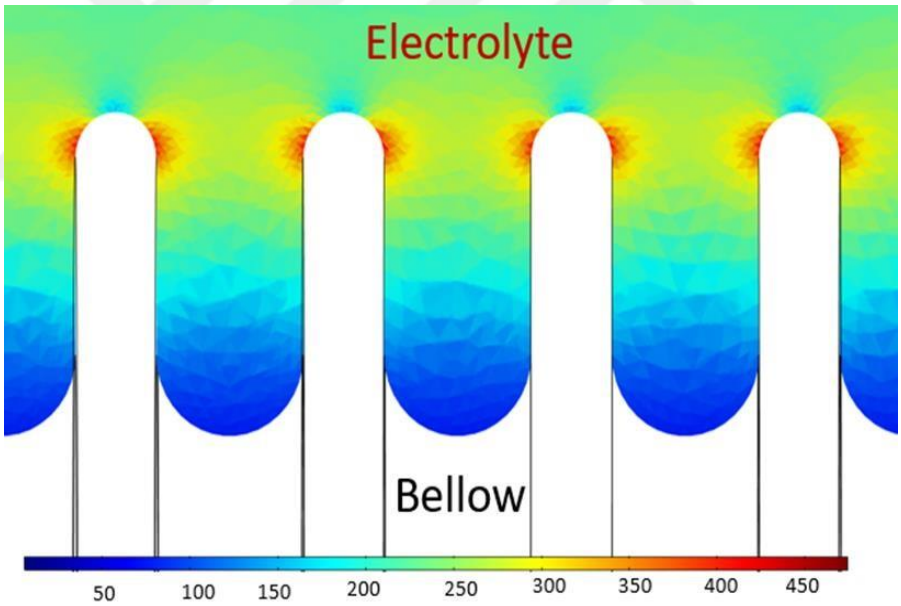


Figure 16 Computer simulation of electroformed bellow by DC method.

At the beginning of the experiments, DC, PC and PRC methods were compared to obtain the finest grain size, the highest hardness and the most homogeneous thickness distribution. The same (average) current density (2 A/dm^2) was applied to observe differences between these three methods.

Figure 17 shows the microstructures of nickel electroplating on copper using different techniques. As it is shown, PRC method provided finer grain size compared to other methods.

Finer grain size provides enhanced mechanical properties such as high hardness, wear and corrosion resistance [31]. The relation between grain size and hardness was modelled by Petch and Hall [44]. Eq. 27 is the expression of this relation:

$$H = H_o + K_H \frac{1}{\sqrt{d}} \tag{27}$$

where d indicates grain size and H is hardness. H_o and K_H are calculated experimentally for the specific metals [45]. As seen in Eq.27, hardness value is inversely proportional to grain size of the metal.

Another difference between DC and PRC methods was orientation of atoms. The orientations of atoms were obtained by XRD analyses which are shown in Figure 18. When nickel was electrodeposited by DC method, preferred orientation was (111). It had pyramidal grains as shown in Figure 19.a. which shows Figure 17.a at higher magnification. But when PRC was used, preferred orientation became (200). This orientation showed globular grains as shown in Figure 19 .b which provided a smoother surface.

In addition to enhanced mechanical properties, finer grains provided better surface properties; it became brightener and smoother. In Figure 20, the surface of the nickel electrodepositions which were coated by different methods are demonstrated.

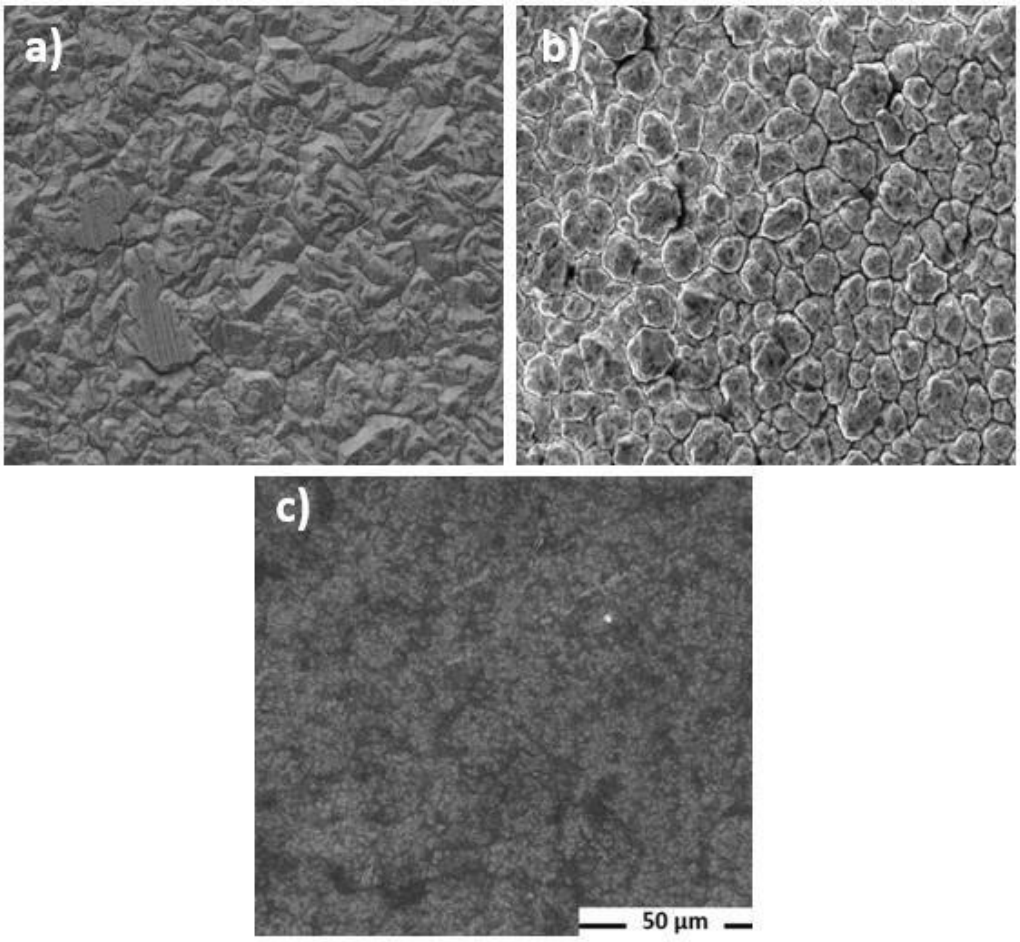


Figure 17 SEM images of nickel electrodeposition by (a) DC (b) PC (I_{ON}=5A/dm^2 , t_{ON}= 2 ms, t_{OFF}= 3 ms) and (c) PRC (I_{CC}=20 A/dm^2, t_{CC}= 3 ms, I_{AA}=20 A/dm^2, t_{AA}=1 ms and t_{OFF}=16 ms) method at a current density of 2 A/dm^2. The scale at the bottom applies to all.

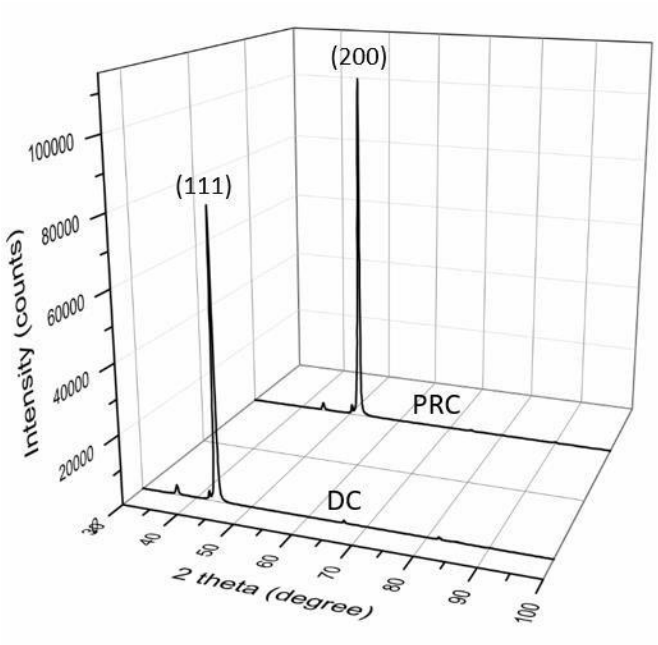


Figure 18 XRD results of nickel electrodeposition with DC and PRC methods.

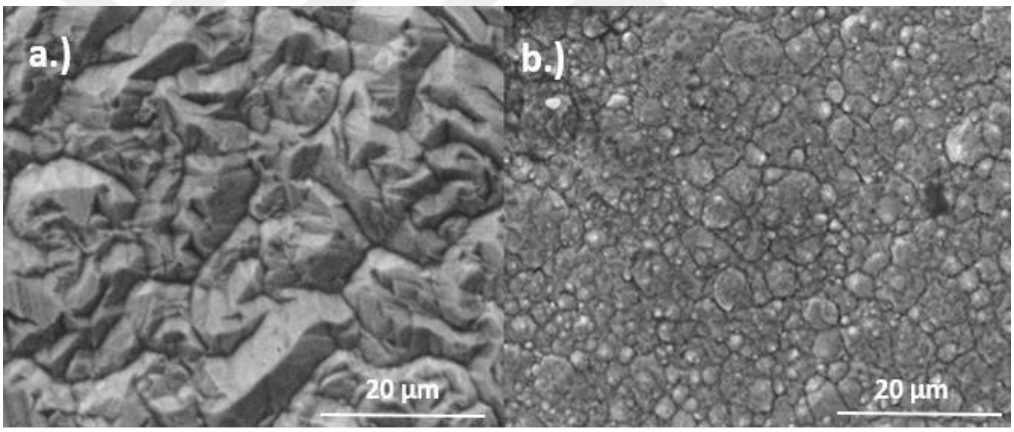


Figure 19 SEM images of nickel electrodeposition (a.) DC (2 A/dm^2) (b.) PRC (I_{CC}=5 A/dm^2, t_{CC}= 3 ms, I_{AA}=2 A/dm^2, t_{AA}=1 ms and t_{OFF}=2.5 ms).

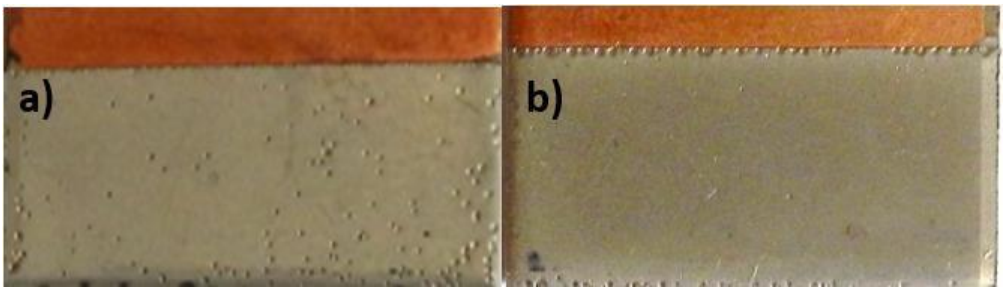


Figure 20 The surface of nickel electrodeposition by a.) DC (1.5 A/dm^2) and b.)PRC method (I_{CC}=20 A/dm^2, t_{CC}= 0.3 ms, I_{AA}=20 A/dm^2, t_{AA}=0.1 ms and t_{OFF}=2.3 ms).

4.2 Effect of Average Current Density on Microstructure and Hardness

The quality of electroforming mainly depends on microstructure and mechanical properties. Grain size of the electrodeposition has attracted great attention due to fine grain strengthening mechanism. According to fine grain strengthening mechanism, grain boundaries prevent dislocation motion in the polycrystalline structure. This inverse relation between strength and grain size was previously given in equation 27.

In the scope of the project, grain sizes were measured by SEM. Effects of each parameter on grain size was compared separately. Firstly, average current density was examined to obtain finer grain size and higher hardness value. Pulse and reverse current densities and their application durations were kept constant to evaluate average current density effect. Nucleation and growth of electrodeposition theory explains relation between overpotential and nucleation rate. It is known that when higher current density is applied, overpotential increases (Eq.28). It means higher current density provides higher nucleation rate and grain refinement [46].

$$\ln v = A - \frac{B}{\eta^2} \tag{28}$$

where v is nucleation rate, η is the overpotential and A and B are constants. Despite this theory, finest grain size was observed at the lowest average current density (1 A/dm^2) in this study. As can be seen in SEM images shown in Figure 21, grain size increased with an increase in average current density. It can be explained with behavior of inhibition species (H_2 and $Ni(OH)_2$ etc.) which impede grain growth. Adsorption of inhibiting species decreased when current density increased. Thereby, grains grow more and became coarser [47]. In addition, high current density may cause inadequate Ni ion transformation from nickel-electrolyte interphase which may decrease nucleation rate [34].

When studying the influence of average current density on microstructure, only t_{off} was changed to adjust average current density. The t_{off} was at its highest value of 1 A/dm^2. During off time, electron double layer discharges completely [48]. This situation provides better ion transfer and higher nucleation rate, so finer grain size is obtained.

Orientation of the electrodeposited nickel was evaluated by XRD and Figure 22 shows that the intensity of preferred orientation changed with average current density. As mentioned

previously, (200) is the most seen orientation in pulse method [50]. The preferred orientation (200) can be called as “free growth mode”, because there is no undesired chemical inhibition due to the off time which gives a chance to desorption of adsorbed inhibition species and impurities [50]. The intensity of preferred orientation is in direct proportion to grain size of the electrodeposition [49]. Higher average current densities increased the intensity of (200) peak, because adsorbed hydrogen (H_{ads}) concentration is reduced, due to higher over-potential [39].

In addition to XRD analyses and SEM images, hardness measurements have a great importance in the characterization of electroplated structures. The relation between average current density and hardness is shown in Figure 23. The points given in this figure were obtained by taking the average of five randomly measured hardness values from the surface. The hardest nickel electrodeposition was obtained at 1 A/dm^2. In addition to larger grains, higher average current densities cause higher voltages which lead to hydrogen evolution at the cathode. These hydrogen bubbles cause pitting at the surface. The change in hydrogen bubble formation (pitting) with current density is imaged in Figure 24. As it is seen, in addition to increase in pitting, dendritic growth occurred on the sharp edges of the specimen at the higher current density. Throwing power also deteriorated at high voltage systems. Higher voltage causes dendritic growth at sharp regions and non-equal thickness distribution [50].

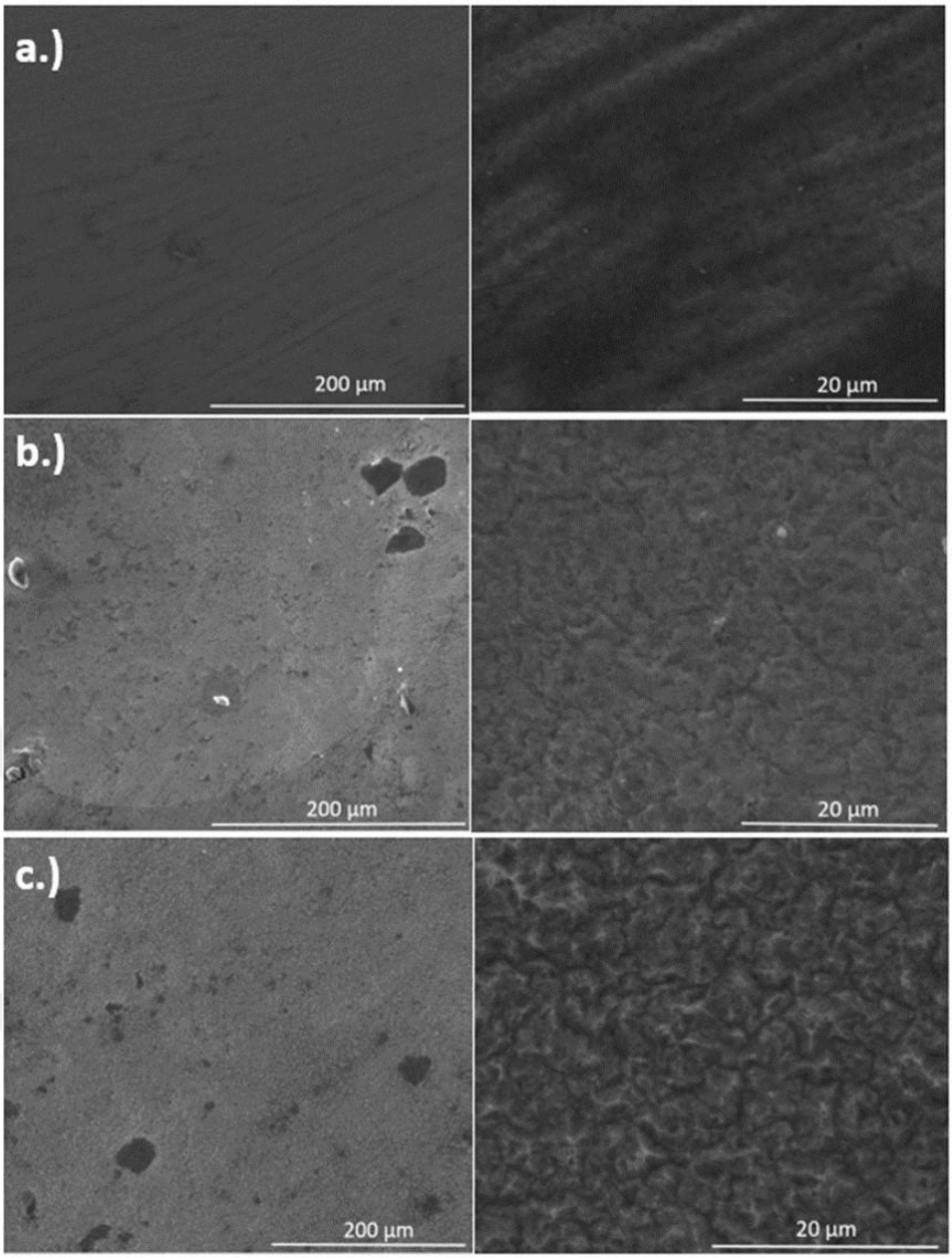


Figure 21 Microstructures of nickel electrodeposited at average current densities of; a.) 1 A/dm^2, b.) 3 A/dm^2, and c.) 5 A/dm^2 at different magnifications.

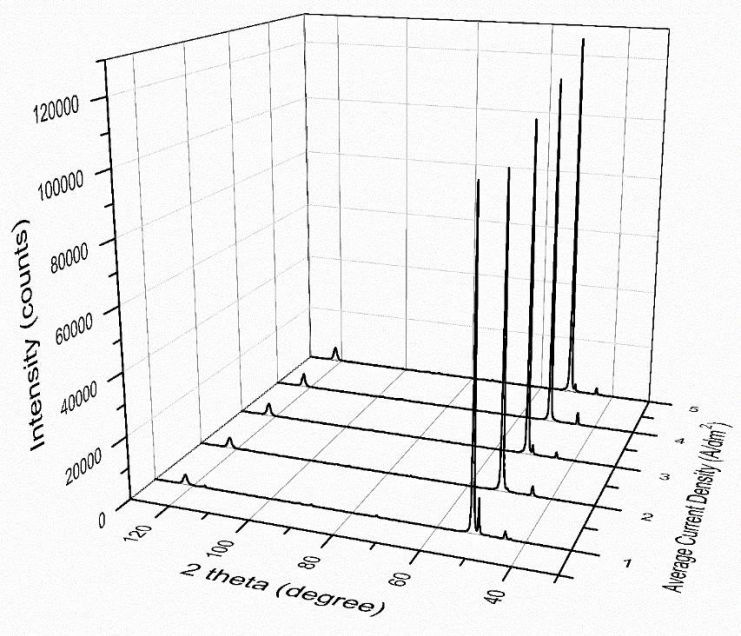


Figure 22 XRD results of nickel electrodeposited at different average current densities.

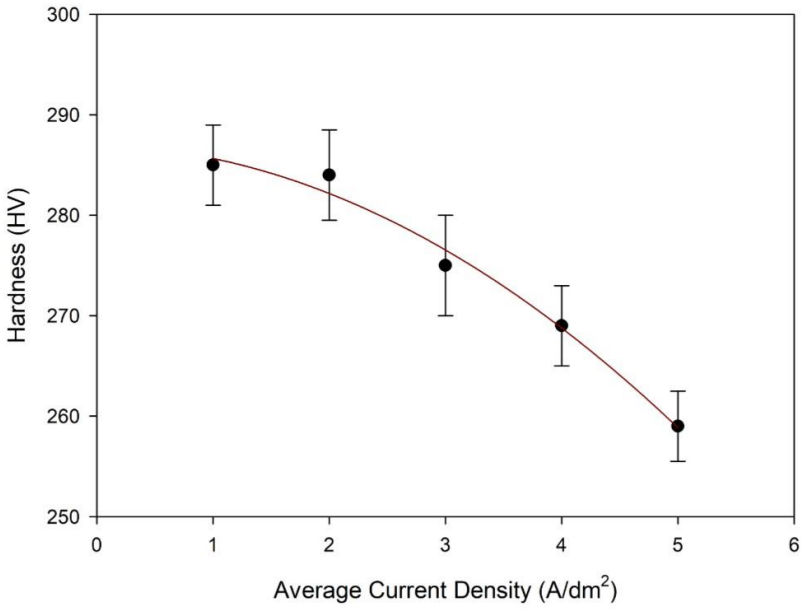


Figure 23 Hardness values of nickel electrodeposited at different average current densities.

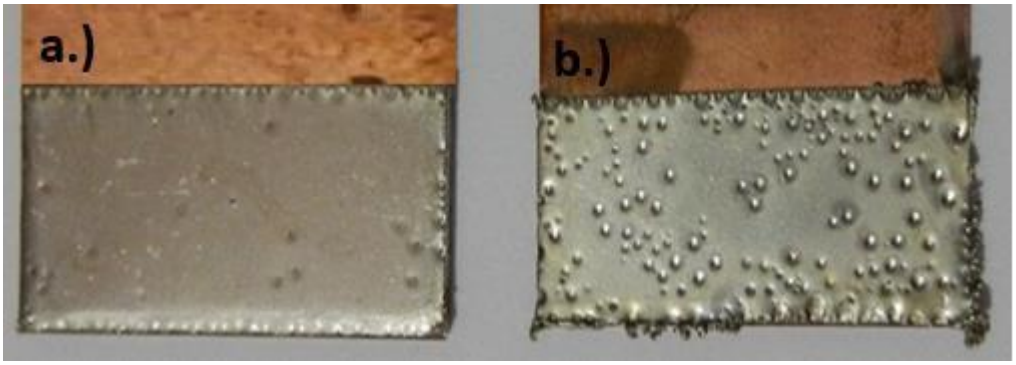


Figure 24 Images of nickel electrodeposition at; a) 1 A/dm^2 and b) 5 A/dm^2 average current densities.

The optimization of average current density was carried out by considering physical and mechanical properties. The lowest average current density was much desirable to obtain the best physical and mechanical properties. On the other hand, a 200 micron electroform structure can be obtained in 34 hours at 1 A/dm^2. In addition, metallic impurities in the electrolyte can be deposited with nickel at low current densities. Because of these reasons, 1.5 A/dm^2 was taken as the optimized average current density.

4.3 Effect of Peak Current Density on Microstructure and Hardness

The advantage of the PRC method is that, there are more current parameters to play with. In this part, anodic and cathodic current densities applied were equal and adjusted between 20 and 120 A/dm^2. Cathodic time was set as 0.3 and anodic time was 0.1 ms. The average current density could be kept constant at 1.5 A/dm^2, by arranging t_{off} values accordingly. SEM micrographs of nickel electrodeposits at 40, 70 and 120 A/dm^2 are given in Figure 25. As it can be seen in this figure, extremely fine grain size was obtained.

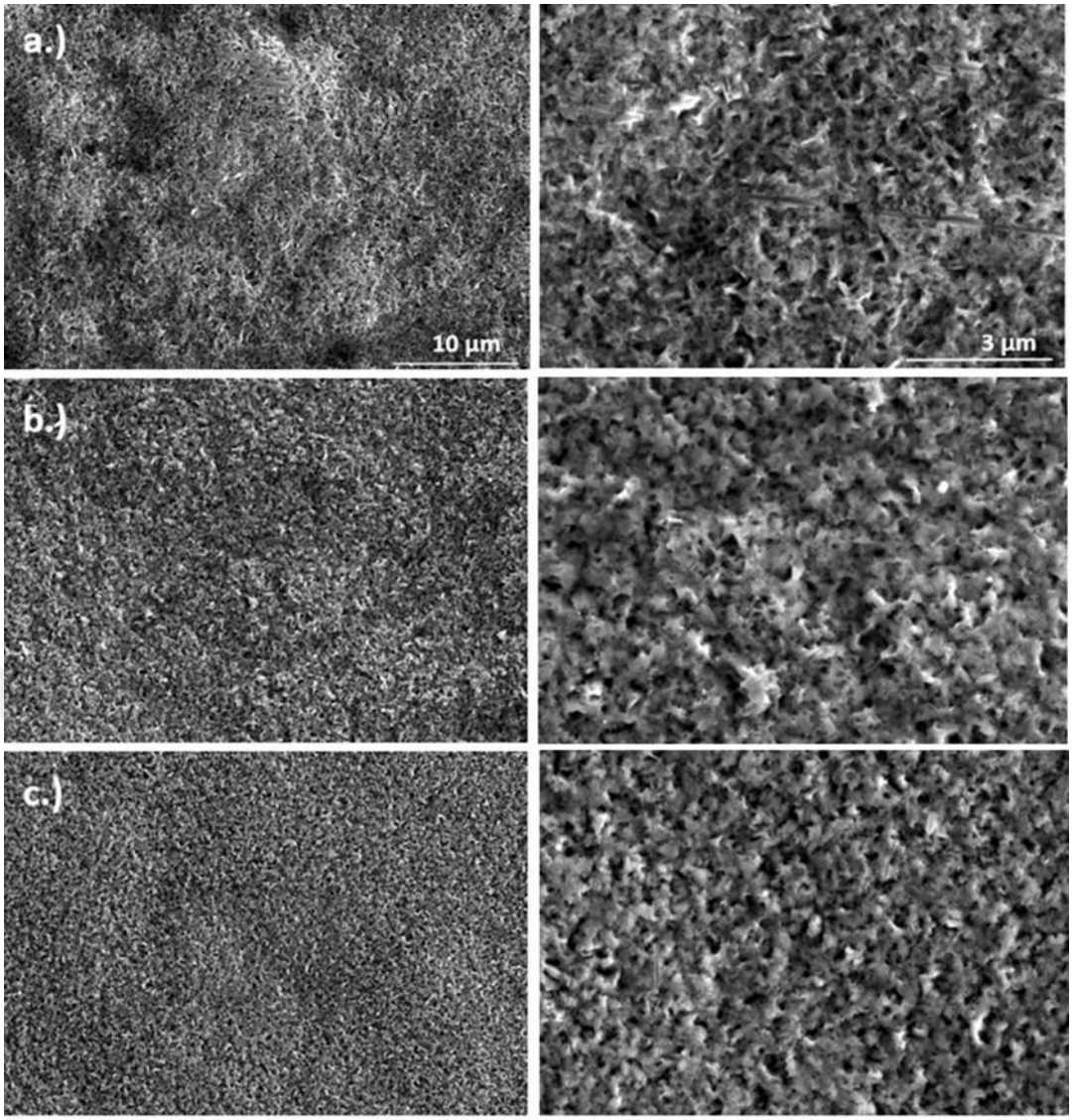


Figure 25 SEM images of nickel electrodepositions at different peak current densities; a.) 40 A/dm^2, b.) 70 A/dm^2, c.) 120 A/dm^2. The scale at the top applies to all.

Figure 26 shows XRD results of the samples. The preferred orientation was observed as (200) for all samples due to PRC method. When intensities of (200) peaks were compared, the lowest intensity was obtained at 120 A/dm^2. It is known that higher peak current densities increase the

nucleation rate [6]. It suddenly increased atom population and ion concentration, so very fine grain size was obtained. On the other hand, the highest t_{off} was applied at 120 A/dm^2 to keep the average current density at 1.5 A/dm^2. High relaxation time (t_{off}) enables discharge of the electron double layer which hinders ion transfer from electrolyte to electrode surface. This positive effect of t_{off} also increases nucleation rate [48].

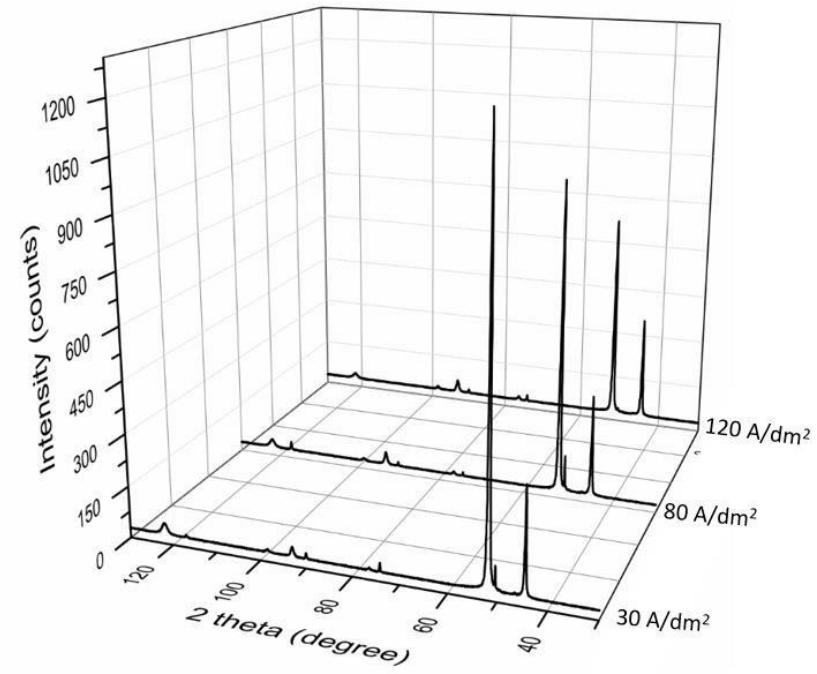


Figure 26 XRD results of nickel electrodeposited samples at different peak current densities.

Long off time not only provides grain refinement but also avoids adsorption of some undesired species onto the cathode surface, which enhances the surface morphology [51].

The results of hardness measurement of samples are given in Figure 27. The hardness value of electrodeposits gradually increased from 20 A/dm^2 to 120 A/dm^2 as expected according to the Hall-Petch theory [53,46]. Finer grain size makes the metal harder.

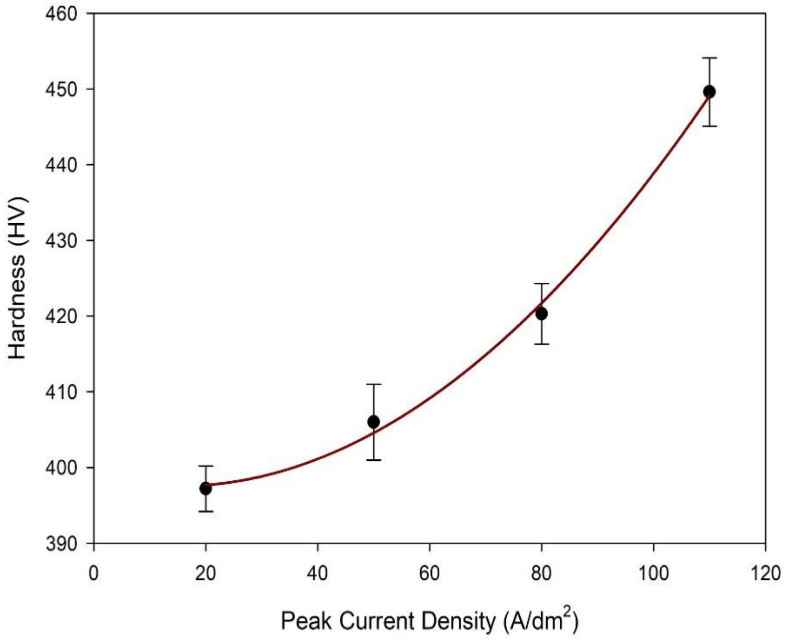


Figure 27 Hardness measurements of electrodeposited nickel at different peak current densities.

4.4 The Effects of Anodic to Cathodic Current Ratio on Microstructure and Hardness

The ratio between anodic current and cathodic current was investigated in this section. Finest grain size was obtained at 120 A/dm^2 peak current density, but the voltage limit of the power source was not capable of applying 120 A/dm^2 current density over 17 cm^2 surface area of accordion geometry. For this reason current density was decreased to 70 A/dm^2 and this value was applied during electroforming the accordion geometry. However, it was noticed that throwing power deteriorated even at such peak current density. Therefore 20 A/dm^2 was used as an optimized peak current density.

In all experiments, cathodic and anodic times were set as 0.3 and 0.1, respectively. Firstly, cathodic peak current density was kept constant at 20 A/dm^2 and anodic current density was changed proportionally.

In the second part of the experiments, 20 A/dm^2 was applied as the anodic current density and cathodic current density was changed proportionally. In both cases, average current density was kept constant at 1.5 A/dm^2 by changing t_{off}. For this parameter, the thickness distribution was also investigated. Firstly, coupon based experiments were done to get better mechanical

properties and then selected parameters were applied to accordion geometry. Figure 28 represents the hardness of electrodeposition for different ratios. The hardest metal electrodeposition was obtained when the ratio of anodic to cathodic current was 0.6 within the parameter range covered in this study. Figure 29 shows microstructures of both cases: higher cathodic current density and higher anodic current density. There are significant differences between these microstructures. When the cathodic to anodic ratio was 0.6. very coarse grain size was formed. Otherwise, very fine grain size and smooth surface were observed. It can be related to the fact that high anodic current can cause formation of undesired species. To verify this prediction, electrodeposits were analyzed by energy dispersive spectroscopy (EDS). Although pure nickel was observed at lower anodic current density, 1.72 wt. % chloride and 0.52 wt. % sulphur were detected at higher anodic current density. Probably, high positive current on cathode caused $NiCl_2$ formation in electrodeposition.

In addition to the EDS analysis and SEM images, XRD analyses were performed to investigate texture of nickel. Figure 30 shows the XRD results. Although predominant peak was (200) for both cases, (220) peak appeared for the second case and the intensity of (200) peak of second case was ten times lower than first case. This is because inhibition species causes non-homogeneous orientation. Thanks to these analyses, higher cathodic current density was selected as a better option for electrodeposition process. This information was used, when the complex accordion geometry was coated.

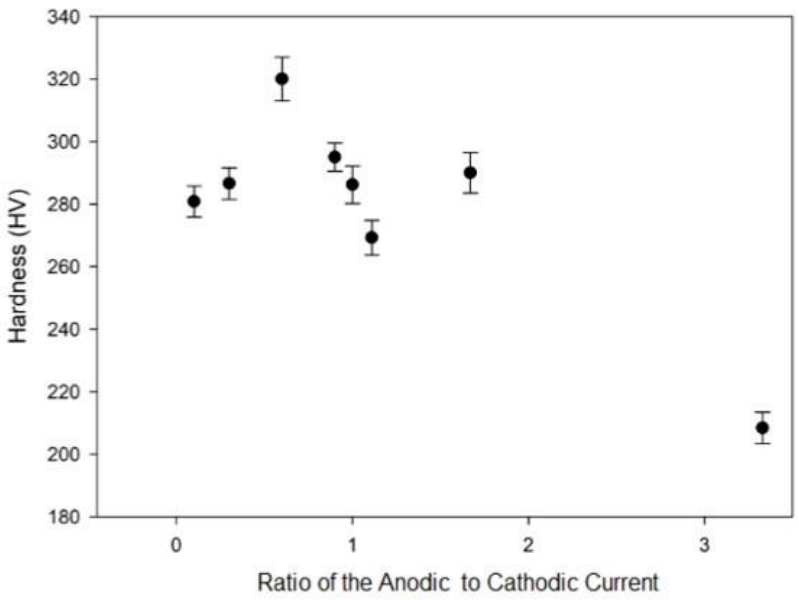


Figure 28 Hardness of nickel electrodepositions for different anodic to cathodic current ratios.

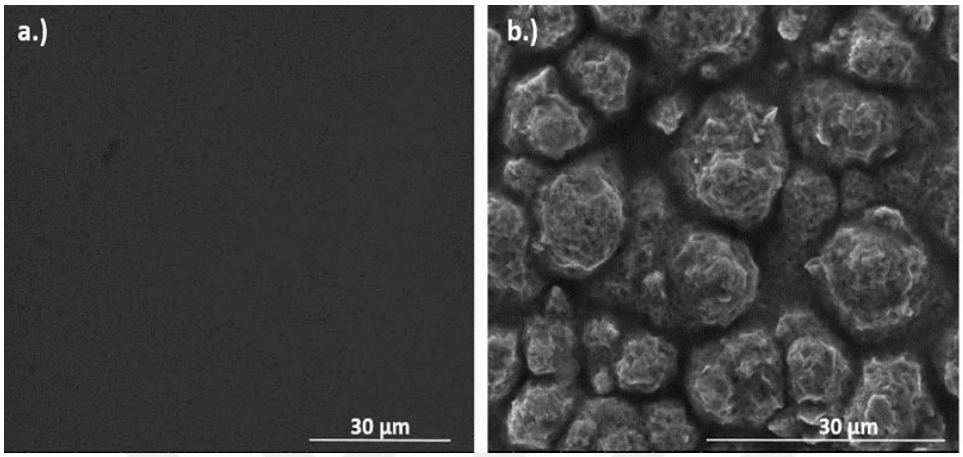


Figure 29 SEM images of of nickel electrodeposition when a.) $\frac{\text{anodic current}}{\text{cathodic current}}=0.6$, b.) $\frac{\text{cathodic current}}{\text{anodic current}}=0.6$.

In the second part of the experiments, the effect of the ratio on thickness distribution was observed. Accordion geometry was used within the scope of this part of the experiments. Figure 31 shows the cross section of accordion geometry, where significant differences between inner and outer thicknesses are present. The results of the thickness measurements are listed in Table 6. When the perfect distribution is obtained, ratio of inner thickness to outer thickness (%) should be 100 which is extremely difficult to achieve practically. The best result obtained was 14.3% at an cathodic to anodic ratio of 0.5, which was not satisfactory for engineering applications. To enhance thickness homogeneity between prominent and recessed regions, a mask was used in front of the cathode. When the mask was used in combination with PRC method, the ratio of inner thickness to outer thickness became 54%, as shown in Figure 32.

4.5 Introduction of Elastic Properties

High elasticity is another desired property for below type sensors. It should be able to expand under high pressure without any plastic deformation and crack formation. To further improve elasticity of the electroform structure, two different approaches were investigated on bellows

formed under optimized plating parameters. They are; the use of S-anodes (sulphur containing nickel) and formation of Ni-Co alloy instead of pure nickel structures.

4.5.1 Use of S-Anodes in Non-chloride Sulphamate Bath

Solution contents and anode types were investigated to obtain higher elasticity. Some studies claimed that nickel chloride increases the stress of the electrodeposits and makes it more brittle [52–55]. It is also known that the most important role of nickel chloride is to prevent anode passivation and increase efficiency. When polarized nickel (S-anode) anodes are used in sulphamate baths, there is no necessity for nickel chloride to activate the anodes [52–55].

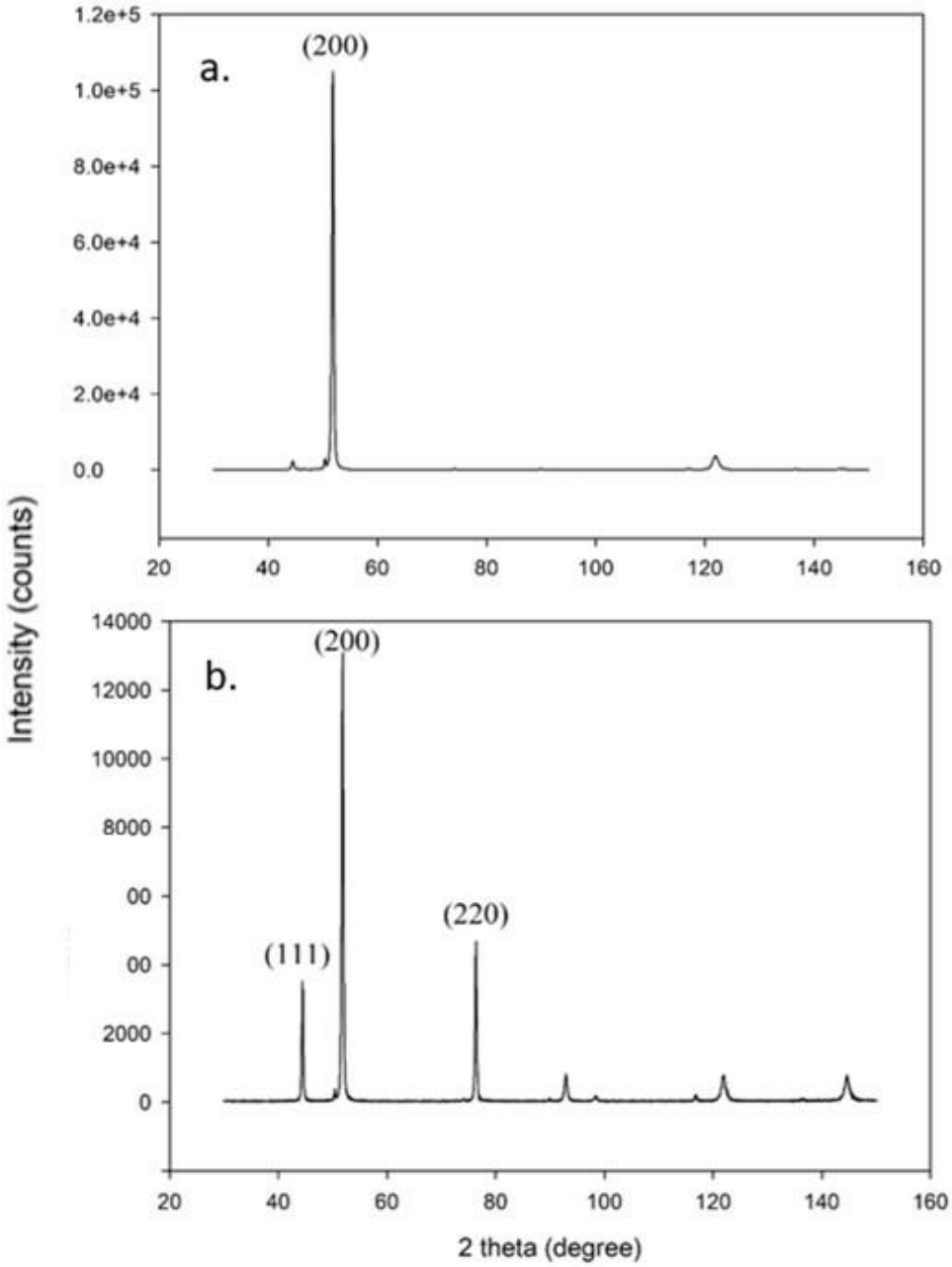


Figure 30 The X-ray diffraction of nickel electrodeposition at cathodic to anodic current ratios of; a.) $\frac{\text{anodic current}}{\text{cathodic current}} = 0.6$ and b.) $\frac{\text{cathodic current}}{\text{anodic current}} = 0.6$.

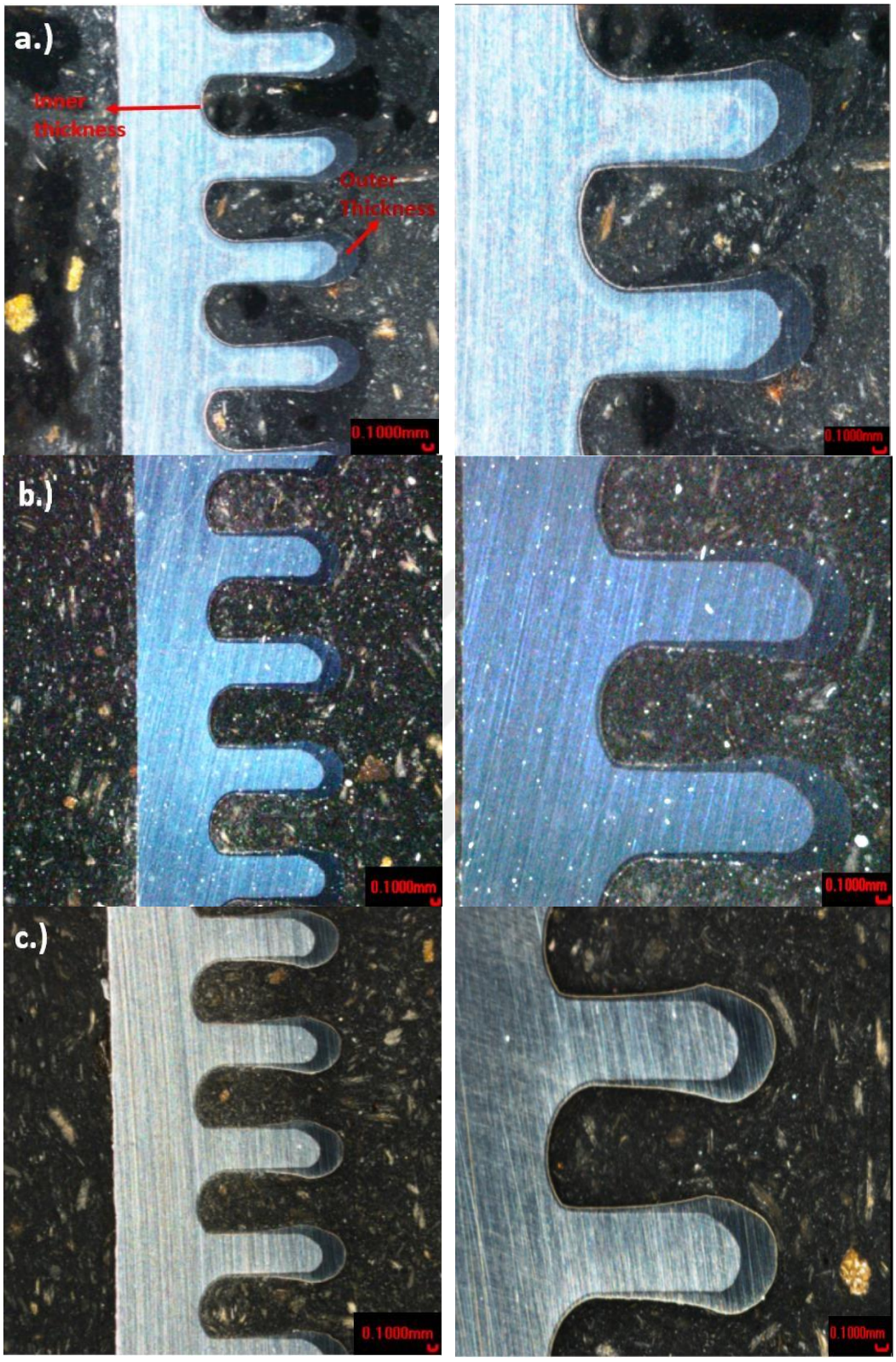


Figure 31 The cross section of the nickel accordion geometry for different ratios of anodic current to cathodic current a.) 0.1, b.) 0.5 and c.) 1.

Table 6 Thickness measurements of nickel electroform with different anodic to cathodic current ratio.

Ratio of Anodic to Cathodic Current	Inner Thickness (μm)	Outer Thickness (μm)	Ratio of Inner Thickness to Outer Thickness (%)
0.10	23.30	296.71	7.85
0.50	41.75	291.07	14.30
1.00	31.27	305.18	10.25

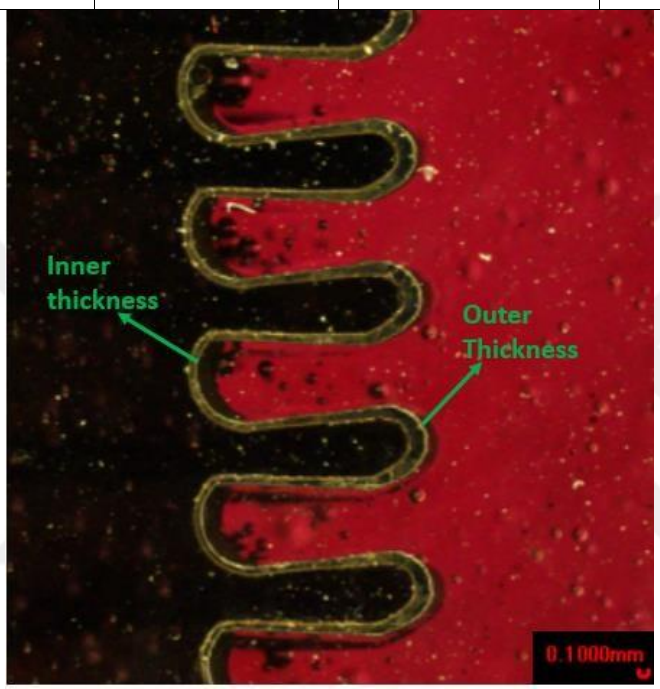


Figure 32 The thickness distribution of nickel electrodeposits when the mask and PRC (I_{CC}= 20 A/dm^2, t_{CC}= 0.3 ms, I_{AA}= 10 A/dm^2, t_{AA}=0.1 ms and t_{off}= 2.8 ms) were used together.

Using non-chloride electrolyte with S-anode decrease the internal stress of accordion geometry. The stress of the electroformed structure was evaluated applying force with hand. There was no cracking and shape deformation, after electroform was compressed and expanded, but there was some question about sulphur contamination. S-anode, also called as sulphurizied nickel anode, includes essential amount of sulphur. For large scale applications, they are placed in large titanium baskets and covered by cloth anode bags. These bags avoid nickel sulphide residue entering into the electroplating solution. In the present study, only a small piece of an anode was

used because of the small surface area of the mandrel. So titanium baskets and anode bags were not used. Absence of anode bags caused some undesired precipitation under some parameters.

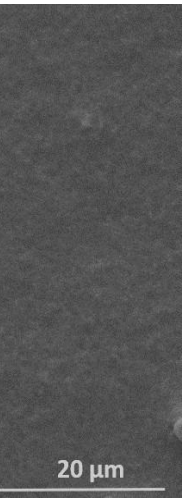
After all of these inferences, a new experiment set was designed to get a more elastic electroform structure without any residue. As can be seen from the experimental design given in Table 7, only off time was investigated. Other parameters were kept constant when t_{off} was changing, which means each sample was deposited at a different average current density. Main purpose was to observe the change in the surface morphology and determine the appropriate parameters to get nickel electrodeposition without sulphur.

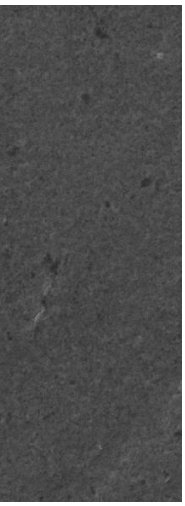
Figure 33 includes microstructures of S-anode based experiments. It was noted in literature that long off time promotes desorption of inhibition species [51]. In the view of this information, EDS analyses were done to investigate undesired species. Pure nickel depositions were observed until t_{off} was dropped to 12 ms. The detected sulphur levels were 0.44 wt % at t_{off} =12 ms and 0.93 wt. % at t_{off} =9 ms. It indicates that relaxation time was insufficient for desorption of sulphur from these two samples. SEM images given in Figure 33 reveal the structural effect of sulfur to the deposits. First four deposits had smoother surfaces with very small grain sizes. However, grains started to become coarser at t_{off} =12 ms. As a result, it was decided that t_{off} should not be shorter than 15 ms to get a good deposit.

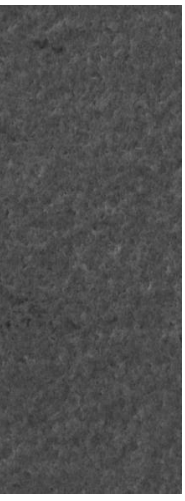
Table 7 Coupon based experiments employing S-anode.

I_{CC} (A/dm^2)	t_{CC} (ms)	I_{AA} (A/dm^2)	t_{AA} (ms)	t_{off} (ms)
20	3	20	1	24
20	3	20	1	21
20	3	20	1	18
20	3	20	1	15

20	3	20	1	12
20	3	20	1	9


20 µm





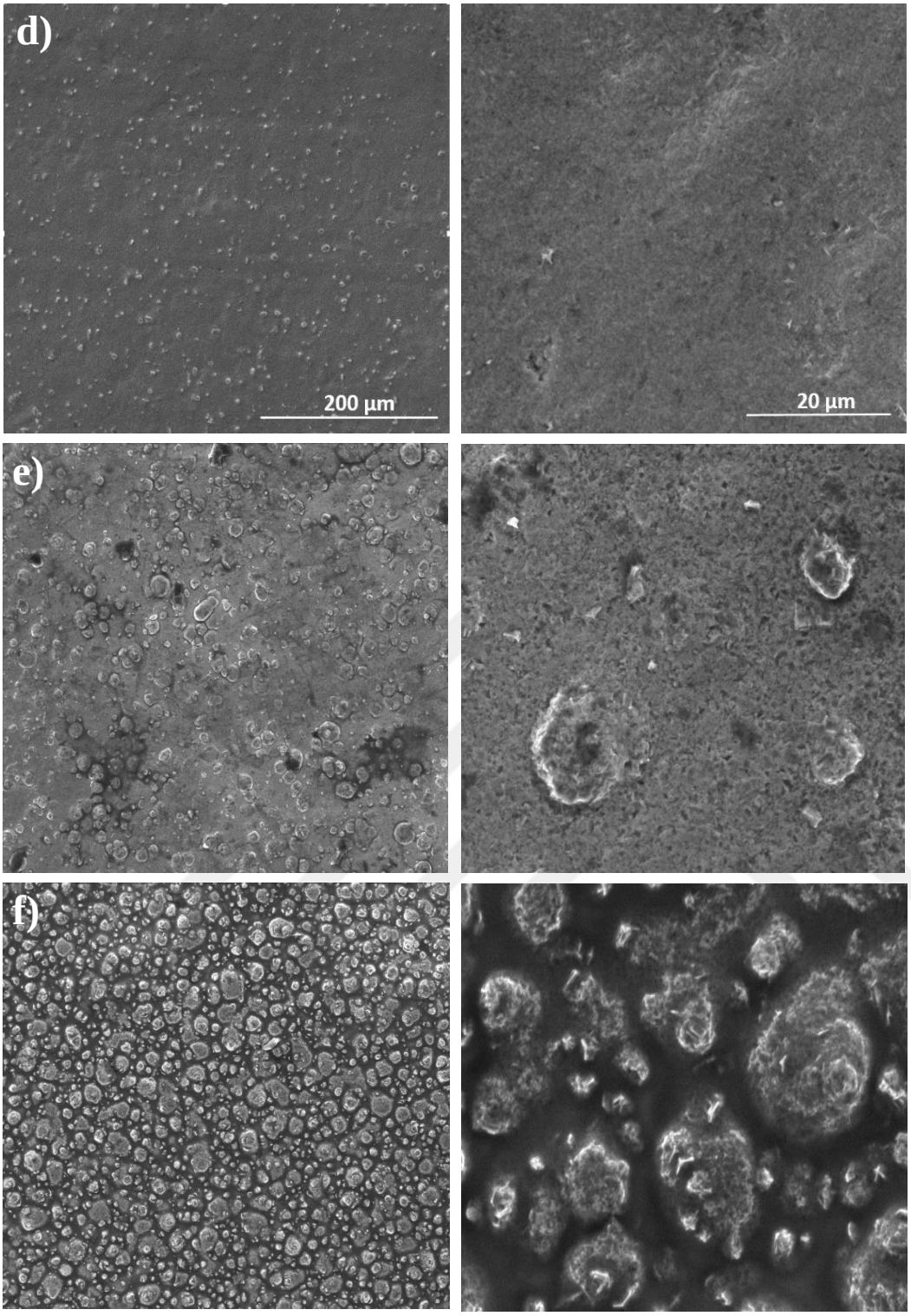


Figure 33 SEM images of nickel electrodeposits at different t_{off} a) 24 ms b) 21ms c) 18 ms d) 15 ms e) 12 ms and f) 9 ms The scale at the top applies to all given at two different magnifications.

Additionally, hardness results are given in Figure 34. As it was expected there was an inverse relationship between hardness values of electrodeposits and t_{off}. Hardness was directly related to grain size.

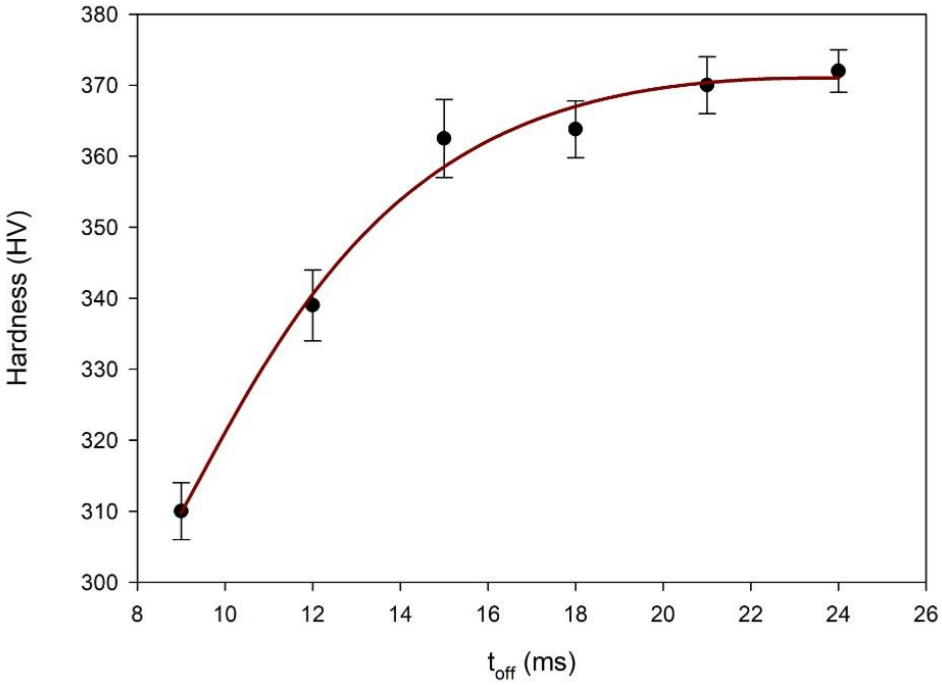


Figure 34 Hardness values of nickel electrodeposits for different off times.

4.5.2 Ni-Co Alloy Plating and Heat Treatment

There are several studies about the effect of cobalt on mechanical properties of nickelcobalt alloys in literature [53, 56–60]. These studies show that nickel cobalt alloys have better hardness and strength compared to pure electrodeposited nickel, because cobalt acts as a microstructure refiner and decrease additive usage [53, 56–60]. Studies claim that carbon, nitrogen and sulfur can precipitate at grain boundaries of the nickel electrodeposits which limit the ductility and ultimate tensile strength (UTS) [63, 64]. The precipitation can be avoided by cobalt, especially at high temperatures [63-65]. Especially, the study of Stein and his colleagues [65] was mainly about heat treatment effect on obtaining high strength and elastic nickel cobalt alloys. In the light of these studies, different cobalt percentages and five heat treatment temperatures were investigated to form a highly elastic bellow structure. The furnace was heated to the target temperature at a ramp rate of 10^{o}C/min and 1 hour of dwell time. Results are listed in Table 8. Figure 35 shows tensile test specimens which were prepared by electroforming and cut by a water jet.



Figure 35 Tensile test specimens for Ni-Co alloys.

Tensile test results are given in Figure 36 and Figure 37. These results provided important information about the mechanical properties of nickel-cobalt alloy electroforms, as elasticity being the most crucial property within the scope of this study. In addition to the elasticity, strength is another important property for high quality bellow type sensors because they must have sufficient strength to withstand the high pressures. As it is shown in Figure 36 and Figure 37, strength of the alloy

electrodeposition significantly dropped at high temperature (600°C and 700°C) heat treatments. Tensile strength was measured as 478.68 MPa for 3% cobalt samples heat treated at 300°C. On the other hand, for the same cobalt fraction, tensile strength was 102.62 MPa when heat treatment was applied at 700°C. A similar behaviour was observed for %4 cobalt alloy. Its tensile strength was 480.53 MPa and 182.31 MPa when heat treatments were at 300 and 700°C respectively. Therefore, it was concluded that (3 and 4% cobalt), heat treatments at 600 and 700^{o}C decreased the strength of the alloy electroform too much. Therefore, heat treatment procedures at other temperatures were considered for optimum strength and elasticity combination. For this purpose, each stress-strain graph was separately drawn and a line was taken from 0.2 % offset point to yield strength to find elastic modulus of the material [66]. Similar mechanical behaviors of 3% and 4% cobalt alloys can be seen in Table 8. Additionally, for both cases, there were two points which may be attributed to lower yields at 500 and 600 °C.

Elastic modulus can be basically described as a material's resistance to elastic deformation [67]. This means lower elastic modulus provides better elastic behavior. According to Table 8, after eliminating heat treatment at 600 and 700°C because of low yield strength, the lowest elastic modulus was observed at 500°C for both cobalt percentages. Higher yield strength was obtained for 3% cobalt at 500°C. In the view of these results, 3% cobalt nickel alloy electroform heat treated at 500°C for 1 hour was considered to yield better mechanical properties.

Table 8 The results of tensile tests for electroformed Ni-Co alloys heat treated at different temperatures.

Cobalt Percentage (wt%)	Temperature (°C)	Elastic Modulus (GPa)	Yield Strength (MPa)
3%	300	41.25	478.68
	400	39.38	374.92
	500	21.61	371.54
	600	18.13	143.23
	700	6.28	102.62
4%	300	41.70	480.53
	400	32.68	365.07
	500	22.80	323.30
	600	15.92	142.97
	700	11.60	182.31

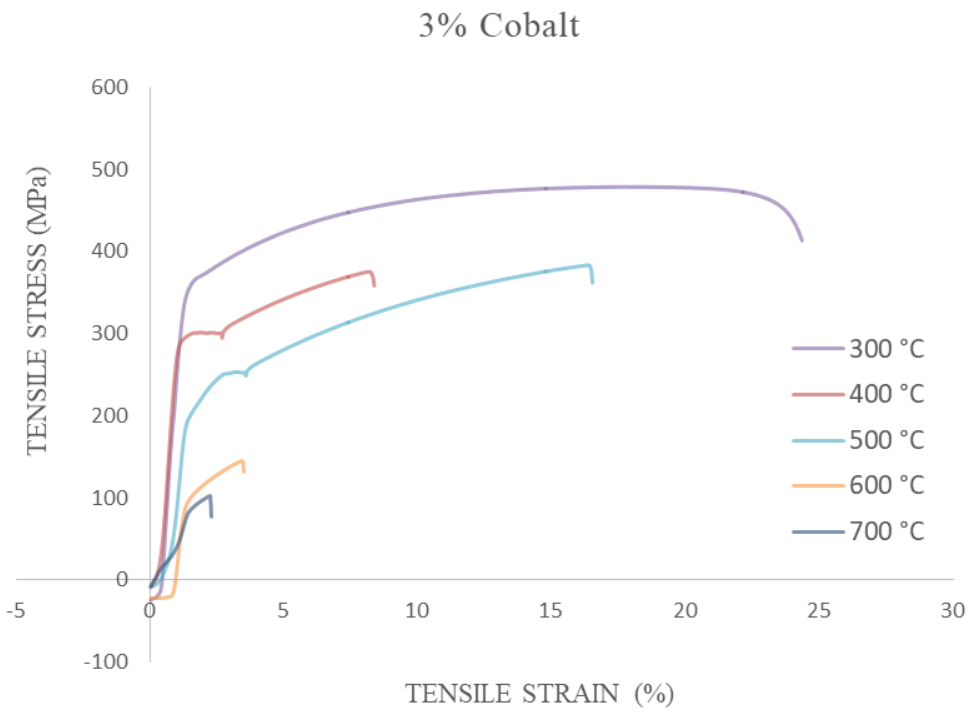


Figure 36 Tensile stress vs strain graphs of 3% Cobalt alloy heat treated at different temperatures.

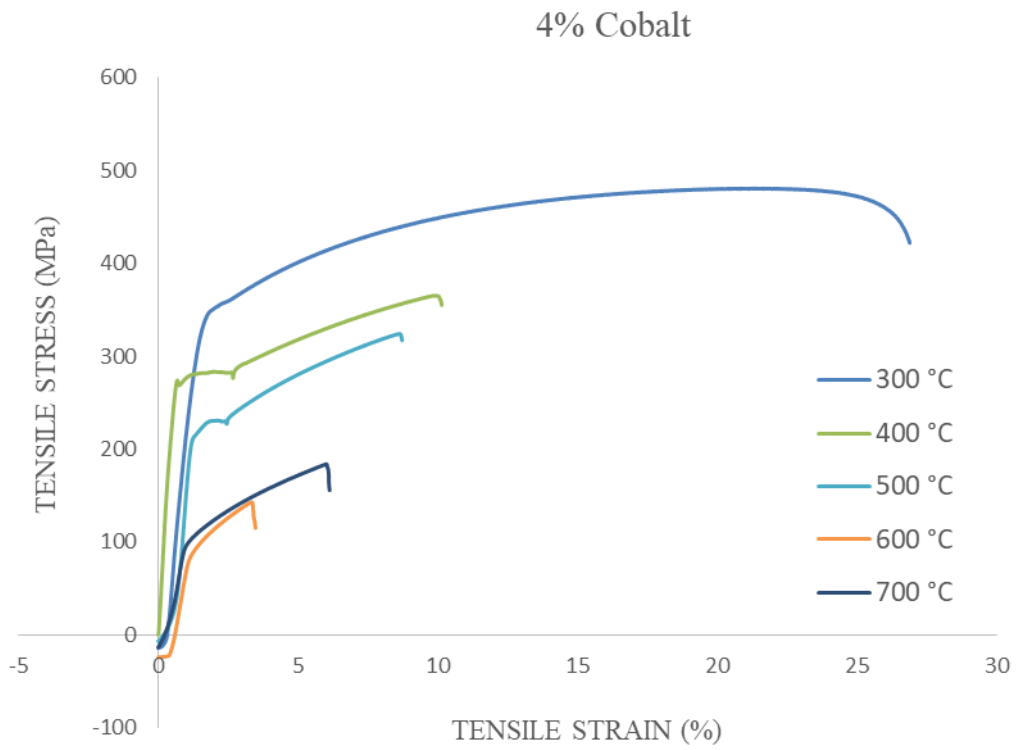


Figure 37 Tensile stress vs strain graphs of 4% Cobalt alloy heat treated at different temperatures.

CHAPTER 5

CONCLUSIONS

Pulse-reverse current parameters and cell design were investigated to enhance mechanical and surface properties of nickel electrodeposition on copper coupons and homogenous current distribution on accordion geometry.

Although lower average current density was found to yield better physical and mechanical properties, 1.5 A/dm^2 was selected as optimum as a result of compromise between properties, duration and contaminations.

The finest grains and the highest hardness values were observed at 120 A/dm^2, which is the highest current density in the limit of the power source. It was not possible to work at the limit due to deteriorations of throwing power over large surface area and 20 A/dm^2 was taken as the optimized peak current density. The hardest nickel electrodeposition was obtained when anodic to cathodic ratio current density was 0.6.

In addition to the mechanical properties, the orientation of electrodeposition was also analyzed by XRD analyses. Preferred orientation was (200) for PRC method. It was observed that the intensity of (200) peak became lower, when finer grain size was obtained.

In this study, another important property was thickness distribution which was studied by changing the ratio of cathodic to anodic current density. The ratio inner to outer thickness (%) became 14% in the case of ratio of cathodic to anodic current density was 0.5. It was thought that this differences was too high for engineering applications, thereby mask was placed in front of cathode to improve homogeneity.

Internal stress was decreased by removing nickel chloride from electrolyte. S-anode was used in non-nickel chloride sulphamate bath to increase anode efficiency.

Elasticity of nickel electroform increased applying heat treatment. 500°C was optimum heat treatment temperature to increase elasticity and yield strength.

REFERENCES

[1] J. A. McGeough, M. C. Leu, K. P. Rajurkar, A. De Silva, and Q. Liu, "Electroforming Process and Application to Micro/Macro Manufacturing," CIRP Ann., vol. 50, pp. 499–514, 2001.

[2] L. J. Durney, Electroplating Engineering Handbook, Berlin: Springer Science & Business Media, 1985.

[3] M. J. Sole, "Electroforming : Methods , Materials , and Merchandise," JOM, vol. 46, pp. 29–35, 1994.

[4] R. Parkinson, "Electroforming: a unique metal fabrication process," AIFM Galvano Tec. e Nuove Finiture(Italy), vol. 9, pp. 140–142, 1999.

[5] Merabellows, 'Basic Materials', [Online], Available: http://www.merrabellows.com/technology/basicmaterials. [Accessed time: 10 December 2017]

[6] G. Y. D. . Z. Giovanni, Theory and Practice of Metal Electrodeposition. New York: Springer, 2011.

[7] F. A. Lowenheim and J. Davis, Modern Electroplating, New jersey: A John Wiley & Sons, Inc., 2010.

[8] M. Sabu,Thomas; Raju, Thomas; Ajesh K, Zachariah; Raghvendra Kumar, Spectroscopic Methods for Nanomaterials Characterization. Cambridge: Elsevier, 2017.

[9] S. B. haji Hasan and D. Sebayang, Electroplating, Rijeka: InTech, 2012.

[10] K. Nasser, Electroplating Basic Principles, Processes and Practice. Berlin: Elsevier, 2004.

[11] J. Bockris and A. Reddy, Modern Electrochemistry 1. New York: Kluwer Academic/Plenum Publishers, 1998.

[12] A. Bard, G. Inzelt, and F. Scholz, Electrochemical Dictionary. Berlin: Springer Science & Business Media, 2012.

[13] C. D. Fern et al., Fundamentals of Electrochemistry , Corrosion and Corrosion Protection. Cham: Springer, 2016.

[14] B. E. Conway and M. A. Sattar, "Study of a Decomposing Hydride Phase at Nickel Cathodes by Measurement of Open-Circuit Potential Decay," vol. 130, pp.
1825–1836, 1968.

[15] M. Paunovic and M. Schlesinger, Fundamentals of Electrochemical Deposition.
New Jersey: John Wiley & Sons,Inc., 2006.

[16] C. Zoski, Handbook of Electrochemistry. Oxford: Elsevier B.V., 2007.

[17] R. Schütze, Micheal Rebak, Raul Bender, Corrosion Resistance of Nickel and Nickel Alloys Against Acids and Lyes, Frankfurt: DECHEMA e.V., 2014.

[18] T. A. Orin, A. Turon, D. Kladekova, and R. M. Smith, "Recent developments in the electrodeposition of nickel and some nickel-based alloys," vol. 36, pp. 957–972, 2006.

[19] ASM International Handbook Volume 5: Surface Engineering. OH: ASM International, 1994.

[20] J. J. Kelly and N. Yang, Electrodeposition of Ni from A Part I . Effect of a Stress Relief on Annealing Behavior and Film Metallurgy, Sand Report,no. October. Sandia National Laboratories, 2001.

[21] P. T. Tang, H. Dylmer and P.Moller “Nickel Coatings and Electroforming Using Pulse Reversal Plating,”, Metal Finishing AESF Electroplating and Surface Finishing, vol.93, pp. 529–536, 1995.

[22] L. J. Durney, Graham’s Electroplating Engineering Handbook, London: Chapman & Hall, 1996.

[23] J. H. Bickford and S. Nassar, Handbook of Bolts and Bolted Joints. New York: Marcel Dekker, 1998.

[24] Z. Abdel-Hamid, “Improving the throwing power of nickel electroplating baths,” Mater. Chem. Phys., vol. 53, pp. 235–238.

[25] T. L. R. Char and S. Sathyanarayana, “Electrodeposition from Sulphamate Solutions,” J. Sci. Ind. Res., vol. 16A, pp. 78–85, 1957.

[26] T. L. R. Char, “Electroplating and Electrorefining of Metals from the Sulphamate Bath,” Electroplating, vol. 11, pp. 343–346, 1958.

[27] Y. Tsuru, M. Nomura, and F. R. Foulkes, “Effects of boric acid on hydrogen evolution and internal stress in films deposited from a nickel sulfamate bath,” J. Appl. Electrochem., vol. 32, pp. 629–634, 2002.

[28] H. C. Rogers, “Hydrogen Embrittlement of Metals,” Science , vol. 159, pp. 1057–1064, 1968.

[29] Nickel Plating Handbook. Nickel Institute, 2013.

[30] M. S. Chandrasekar and M. Pushpavanam, “Pulse and pulse reverse plating — Conceptual , advantages and applications,” vol. 53, pp. 3313–3322, 2008.

[31] L. Shao, L. Du, and L. Wang, “Development of nanocrystalline nickel by pulse reverse microelectroforming,” vol. 5, pp. 165–170, 2010.

[32] N.V. Mandich, HBM Engineering Co., Lansing, IlL, Met. Finish. (2002) .

[33] F. P. Leaman and Jean-Claude, Theory and Practice of Pulse Plating. Orlando: AESF Publication, 1986.

[34] A. Cziraki, L. Pogany, I. Bakonyi, and M. S. Chandrasekar, “Microstructure and electrical transport properties of pulse-plated nanocrystalline nickel electrodeposits,” Electrochim. Acta, vol. 53, pp. 3313–3322, 2008.

[35] Y. Xuetao, W. Yu, S. Dongbai, and Y. Hongying, “Influence of pulse parameters on the microstructure and microhardness of nickel electrodeposits,” vol. 202, pp. 1895–1903, 2008.

[36] A. Chaparro, W. Arnulfo, and E. Vera, “Electrodeposition of nickel plates on copper substrates using PC y PRC,” Rev. Mater., vol. 12, pp. 583–588, 2007.

[37] Y. Y. Eh, C. C. Hen, M. T. Sai, and Y. S. Hyng, “Effect of Pulse-Reverse Current on Microstructure and Properties of Electroformed Nickel – Iron Mold Insert Effect of Pulse-Reverse Current on Microstructure and Properties of Electroformed Nickel – Iron Mold Insert,” Japenese J. Appl. Phys., vol. 44, pp. 1086–1090, 2005.

[38] J. T. Luo, W. B. Lin, and L. Shang, “The Effect of Pulse-Reverse Plating Time on Blind Micro Via Filling Pili,” 3rd Int. Microsystems, Packag. Assem. Circuits Technol. Conf., vol. Taipei, pp. 395–398, 2008.

[39] G. Chul et al., “Effects of Current Density and Frequency on Microstructure and
Mechanical Properties of Ni,” Jpn. J. Appl. Phys., vol. 51, p. 09MJ03-09MJ03-5, 2012.

[40] Y. Tsuru, M. Nomura, and F. R. Foulkes, “Effects of chloride, bromide and iodide ions on internal stress in films deposited during high speed nickel electroplating from a nickel sulfamate bath,” J. Appl. Electrochem., vol. 30, no. 2, pp.
231–238, 2000.

[41] W. E. G. Hansal, B. Tury, M. Halmdienst, M. L. Varsányi, and W. Kautek, "Pulse reverse plating of Ni-Co alloys: Deposition kinetics of Watts, sulfamate and chloride electrolytes," Electrochim. Acta, vol. 52, no. 3, pp. 1145–1151, 2006.

[42] G. E. Totten and D. S. MacKenzie, Eds., Handbook of Aluminum. New York: CRC Press, 2003.

[43] J. Davis, ASM Specialty Handbook, Ohio: ASM International, 2001.

[44] M. Schlesinger and M. Paunovic, Fundamentals of Deposition, New jersey: The electrochemical society series, 2006.

[45] K. P. Wong, K. C. Ã. Chan, and T. M. Yue, "A study of hardness and grain size in pulse current electroforming of nickel using different shaped waveforms," J. Appl. Electrochem., vol. 31, pp. 25–34, 2001.

[46] K. B. Oldham, J. C. Myland, and A. m Bond, Electrochemical Science and Technology Fundamentals and Applications, Chichester: A John Wiley & Sons, Inc., 2012.

[47] A. Czırakı, I. Fogarassy, I. Geröcs, E. Totht-Kadar, and I. Bakonyi, "Microstructure and growth of electrodeposited nanocrystalline nickel foils," J. Mater. Sci., vol. 29, pp. 4771–4777, 1994.

[48] T. Pearson and J. Dennis, "Facts and Fiction about Pulse Plating," Int. J. Surf. Eng. Coatings, vol. 69, pp. 75–79, 1991.

[49] A. Ibanez and E. Fatas, "Mechanical and structural properties of electrodeposited copper and their relation with the electrodeposition parameters," Surf. Coat. Technol., vol. 191, pp. 7–16, 2005.

[50] N. Ibl, Proceedings of A.E.S.F., Int. Pulse Plat. Symp. Rosemont, vol. Illinois, pp. 6–7, 1981.

[51] A. Boukhouiete and J. Creus, “Nickel deposits obtained by continuous and pulsed electrodeposition processes,” J. Mater. Environ. Sci., vol. 6, no. 7, pp. 1840– 1844, 2015.

[52] J. Rösler, H. Harders, and M. Baker, Mechanical Behaviour of Engineering Materials. Mülheim: Springer-Verlag Berlin Heidelberg, 2007.

[53] D. Myron, “Modern Electroforming Solutions and Their Applications,” STP46001S Symp. Electroforming—Applications, Uses, Prop. Electroformed Met., no. 1, pp. 10–31, 2015.

[54] R. C. Barrett, “Nickel Plating from the Sulfamate Bath,” Plating, vol. 41, pp. 1027–1033, 1954.

[55] O. J. Klingenmaier, “The Effect of Anode Efficiency on the Stability of Nickel Sulfamate Solutions,” Plating, vol. 52, pp. 1138–1141.

[56] G. Malone, R. Stauffis, and R. Wood, Nondestructive Tests of Regenerative Chambers. New York: Bell Aerospace Company, 1972.

[57] A. Brenner, Electrodeposition of Alloys PRINCIPLES and PRACTICE, vol. I. New York: Academic Press, 1963.

[58] W. Cruise and R. Walker, “The Use and Production of Electrodeposited Cobalt,” Met. Finish., vol. 76, pp. 45–47, 1978.

[59] W. T. Mcfarlen, “Electroformed Nickel-Cobalt Alloy Deposits: An Evaluation,” Plating, vol. 57, pp. 46–60, 1970.

[60] J. Dini, H. Johnson, and J. Helms, “High Strength Nickel- Cobalt Deposits for Electrojoining Applications,” Rep. SCL-dr-720090, Sandia Lab., pp. 12–26, 1973.

[61] W. B. Stephenson, “Development and Utilization of a High Strength Alloy for Electroforming,” Plating, vol. 53, pp. 183–192, 1966.

[62] Y. Li, H. Jiang, W. Huang, and H. Tian, “Effects of peak current density on the mechanical properties of nanocrystalline Ni – Co alloys produced by pulse electrodeposition,” Appl. Surf. Sci., vol. 254, pp. 6865–6869, 2008.

[63] W. M. Yin, S. H. Whang, and R. A. Mirshams, “Effect of interstitials on tensile strength and creep in nanostructured Ni,” Acta Materalia, vol. 53, pp. 383–392, 2005.

[64] L. Wang, Y. Gao, Q. Xue, H. Liu, and T. Xu, “Microstructure and tribological properties of electrodeposited Ni – Co alloy deposits,” Appl. Surf. Sci., vol. 242, pp.
326–332, 2005.

[65] B. Stein, P. Jaeger, and C. Przybyla, “Mechanical Properties of Electroformed Nickel Cobalt Alloys,” Proc. 22nd Heat Treat. Soc. Conf. and 2nd Int. Surf. Eng. Congr., 2003.

[66] G. Dieter, Mechanical metallurgy, London: McGraw-Hill Book Company, 1962.

[67] M. M. F. Ashby, Materials Selection in Mechanical Design. Burlington: Elsevier, 2011.